GRADIENT DESCENT WITH LARGE STEP SIZES: CHAOS AND FRACTAL CONVERGENCE REGION

Anonymous authors
Paper under double-blind review

ABSTRACT

We examine gradient descent in matrix factorization and show that under large step sizes the parameter space develops a fractal structure. We derive the exact critical step size for convergence in scalar-vector factorization and show that near criticality the selected minimizer depends sensitively on the initialization. Moreover, we show that adding regularization amplifies this sensitivity, generating a fractal boundary between initializations that converge and those that diverge. The analysis extends to general matrix factorization with orthogonal initialization. Our findings reveal that near-critical step sizes induce a chaotic regime of gradient descent where the long-term dynamics are unpredictable and there are no simple implicit biases, such as towards balancedness, minimum norm, or flatness.

1 INTRODUCTION

Understanding the properties of gradient descent in non-convex overparametrized optimization has been a central pursuit in modern machine learning. The step size, or learning rate, is a critical factor determining the dynamics and convergence of gradient descent optimization. In particular, it has a major influence on the returned solution and its generalization performance (Nar and Sastry, 2018; Jastrzebski et al., 2020; Lewkowycz et al., 2020; Cohen et al., 2021). Large step sizes have been associated with flat and balanced minimizers of the training objective (Wu et al., 2018; Wang et al., 2022; Menon, 2024), sparse feature representations (Nacson et al., 2022; Andriushchenko et al., 2023), smooth solution functions (Mulayoff and Michaeli, 2020; Nacson et al., 2023), and improved generalization (Ba et al., 2022; Qiao et al., 2024; Sadrtdinov et al., 2024). Yet, the theoretical understanding of large step sizes remains limited, even in simple convex settings. Our investigation is motivated by two fundamental questions:

Given an initial parameter, what is the critical (largest) step size that allows convergence?

What kind of implicit biases are induced by gradient descent with near-critical step size?

Addressing these questions is challenging, since large step sizes can produce highly complex, non-monotonic, and even chaotic trajectories. In particular, trajectories may not converge to stationary points but instead enter periodic or chaotic oscillations (Chen and Bruna, 2023; Chen et al., 2024b; Ghosh et al., 2025), or converge to a statistical distribution (Kong and Tao, 2020); trajectories that eventually converge to a minimizer may still undergo chaotic oscillations during early training (Zhu et al., 2023; Kreisler et al., 2023; Song and Yun, 2023); and trajectories with nearby initializations can diverge exponentially from one another (Herrmann et al., 2022; Jiménez-González et al., 2025). Moreover, empirically, the set of step sizes and the set of initializations leading to convergence can form fractal structures (see, respectively, Sohl-Dickstein, 2024; Zhu et al., 2023). In this work, we provide precise answers to the above questions in the context of matrix factorization problems with rigorous theoretical characterizations.

We begin by examining gradient descent in a simplified problem to factor a scalar target as the inner product of two vectors. We show that two striking phenomena emerge at large step sizes: (i) trajectories originating from arbitrarily small sets of initializations can converge to global minimizers of the training loss with arbitrarily large norm, sharpness or imbalance, or to a saddle point; and (ii) the set of initializations that converge, that is, the convergence region, has a fractal structure (see the left panel in Figure 1). Thus gradient descent exhibits sensitivity to initialization and its long-term behavior is unpredictable. Interestingly, while the convergence region is regular (in the

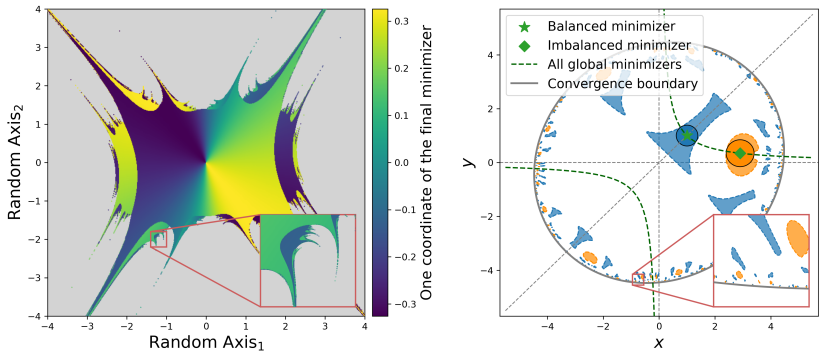

Figure 1: Left: Gradient descent applied to $L(u, v) = (u^\top v - 1)^2 + 0.3(\|u\|_2^2 + \|v\|_2^2)$ with $(u, v) \in \mathbb{R}^{10}$. Shown is a random two-dimensional slice of $\mathbb{R}^{10}$. Gray points are initializations from which the algorithm does not converge; other points are colored by the value of one of the coordinates of the converged minimizer. As we see, the convergence boundary is fractal, and the converged solution depends sensitively on the initialization when this is near the boundary. Right: Gradient descent applied to $L(x, y) = (xy - 1)^2$ with $(x, y) \in \mathbb{R}^2$. The green star marks a balanced minimizer p, with its neighborhood O_p depicted as a blue disk with black boundary. The blue region with dashed boundaries shows the preimage of O_p under GD^6. The green diamond marks an imbalanced minimizer, with its neighborhood and preimages shown in orange. For this problem the convergence boundary is smooth but the convergence point for initializations near the boundary is chaotic.

almost everywhere sense) in the unregularized setting, it becomes fractal once regularization is introduced. Further quantifying the unpredictability of gradient descent, we show that the topological entropy of the gradient descent system is at least $\log 3$. Also, we show that the fractal nature of the boundary of the convergence region is captured by a self-similar curve, whose fractal dimension is estimated as 1.249. To our knowledge, beyond the univariate training loss setting studied by Kong and Tao (2020); Chen et al. (2024b), this is the first rigorous characterization of chaos in gradient descent optimization.

We then extend our analysis to general matrix factorization by showing that, when the initialization lies in a subspace defined by a set of orthogonal conditions, the gradient descent dynamics decouples into several independent scalar factorization dynamics. Hence, all the results established for scalar factorization remain valid and can be applied on this subspace. This includes, in particular, the commonly used identity initialization. Our results also extend to shallow linear residual networks (Hardt and Ma, 2017; Bartlett et al., 2018). We experimentally show that sensitivity to initialization persist over more general settings, such as generic initialization and deep matrix factorization.

We further analyze the mechanisms underlying these phenomena and trace them to a folding behavior of the update map $\mathrm{GD}(\theta) = \theta - \eta\nabla L(\theta)$: the map GD sends a region $\mathcal{C}$ containing multiple minimizers onto a larger region that contains $\mathcal{C}$, in a multi-fold covering manner. As a consequence, for any neighborhood O_p of a minimizer $p \in \mathcal{C}$, the number of connected components in the preimage $\mathrm{GD}^{-N}(O_p)$ grows exponentially with the number of iterations N, and these components accumulate near the boundary of the convergence region. The preimages associated with different minimizers then become intricately interwoven near the boundary, giving rise to sensitive dependence on the initialization and a self-similar fractal structure (see the right panel in Figure 1). Overall, our results show that near-critical step sizes place gradient descent in a chaotic regime, where infinitesimal perturbations on the initial conditions can lead to substantially different training outcomes. This stands in sharp contrast to the stable dynamics observed at smaller step sizes.

1.1 Main Contribution

The goal of this article is to provide rigorous insights into the dynamics of gradient descent with large step sizes in matrix factorization. Our contributions can be summarized as follows:

- We derive the exact critical step size for convergence in scalar factorization and show that, at critical step size, infinitesimal perturbations of the initialization can redirect gradient descent to global

minimizers with arbitrarily large norm, imbalance, or sharpness, or to a saddle. We show that the topological entropy of gradient descent system is at least $\log 3$. We also show that the convergence region in the parameter space is equal almost everywhere to a bounded, smooth domain.

- We show that, with ℓ_2 regularization, gradient descent selects either the minimal distance solution or the maximal distance solution among all global minimizers. Near criticality, infinitesimal perturbations of the initialization can switch this selection from one to the other. We show that if the step size is below an explicit bound, the algorithm always selects the minimal distance solution.
- We show that adding ℓ_2 regularization yields a fractal convergence boundary, whose geometry is captured by a self-similar shape in $\mathbb{R}^2$ after symmetry reduction. We numerically estimate the fractal dimension of this shape. We further show that, up to a measure-zero set, the convergence region has an unbounded interior.
- We extend these results to general matrix factorization under a range of initializations including the identity initialization. We show that gradient descent partitions the parameter space into components where it acts as a covering map, and reason that chaos arises when it is an expansion on a component that contains multiple minimizers.

1.2 Related Work

Gradient Descent Dynamics Under Large Step Sizes A main line of research on large-step-size gradient descent focuses on the non-monotonic convergence of the loss and its impact on the final model. Key perspectives include the *Edge of Stability* (Cohen et al., 2021; Ma et al., 2022; Agarwala et al., 2023; Damian et al., 2023; Ahn et al., 2022; 2023; Zhu et al., 2023; Wang et al., 2023) and the catapult phenomenon (Lewkowycz et al., 2020; Kalra and Barkeshli, 2023; Meltzer and Liu, 2023; Zhu et al., 2024a;b). Compared to these works, our analysis extend to even larger (near-critical) step sizes. Another line of work shows how a large step size can enhance feature learning in one step of gradient descent (Ba et al., 2022; Dandi et al., 2024; Moniri et al., 2025), also comparing different parametrizations (Sonthalia et al., 2025). Similar observations about the role of the step size in feature learning have also been made in SGD (Andriushchenko et al., 2023; Lu et al., 2024) and pre-training (Sadrtdinov et al., 2024). Ziyin et al. (2022) observed that for a certain range of step sizes, SGD can have undesirable behavior, such as convergence to local maxima. For linear networks, Kreisler et al. (2023) identified a monotonically decreasing quantity (sharpness) along the gradient descent trajectories. Wang et al. (2022) showed large step size induces an implicit bias towards balanced minimizers in matrix factorization. Crăciun and Ghoshdastidar (2024) proved the existence of a step size threshold above which the algorithm diverges. Large-step-size gradient descent has also been investigated in logistic regression (Wu and Su, 2023; Wu et al., 2024; Meng et al., 2024), and some of the analysis has been further extended to shallow networks (Cai et al., 2024).

Chaos in Optimization Van Den Doel and Ascher (2012) empirically observed chaos, specifically positive finite-time Lyapunov exponents, for several variants of steepest descent methods. The phenomenon named *period-doubling bifurcation route to chaos* has been widely observed in recent literature (Kong and Tao, 2020; Chen and Bruna, 2023; Chen et al., 2024b; Meng et al., 2024; Danovski et al., 2024; Ghosh et al., 2025). Among them, only Kong and Tao (2020); Chen et al. (2024b) provided rigorous analyses for the chaotic dynamics. They showed the emergence of *Li-Yorke chaos*, i.e., the existence of periodic orbits of arbitrary periods, for univariate training losses. In comparison, our setting is high-dimensional. Additionally, we established not only the existence of all periodic orbits, but also the sensitivity of the limiting point to initialization, which is more relevant to practical optimization, particularly the implicit bias of the optimization algorithm.

2 Preliminaries

We focus on the following shallow matrix factorization problem with ℓ_2 regularization:

$$\min_{\theta=(U,V)} L(\theta) = \frac{1}{2}\left\|U^\top V - Y\right\|_F^2 + \frac{\lambda}{2}(\|U\|_F^2 + \|V\|_F^2), \tag{1}$$

where $\lambda \geq 0$, $U, V \in \mathbb{R}^{d\times d_y}$ and the target matrix $Y \in \mathbb{R}^{d_y \times d_y}$ is a diagonal matrix. The diagonality of Y is a weak assumption that can be achieved by reparametrization. Specifically, for arbitrary Y consider the singular value decomposition $Y = P_Y \Sigma_Y Q_Y^\top$ and the rotations $U = \tilde{U} P_Y^\top$ and

$V = \tilde{V} Q_Y^\top$. The objective then becomes $\tilde{L}(\tilde{U}, \tilde{V}) = \frac{1}{2}\|\tilde{U}^\top \tilde{V} - \Sigma_Y\|_F^2 + \frac{\lambda}{2}(\|\tilde{U}\|_F^2 + \|\tilde{V}\|_F^2)$, where the target is diagonal. Moreover, the optimization dynamics in minimizing $\tilde{L}(\tilde{U}, \tilde{V})$ is identical to those in minimizing $L(U, V)$ up to the rotation (see details in Appendix C).

Gradient optimization in problem (1) has been extensively studied, especially in small-step-size regimes (see, e.g., Saxe et al., 2013; Arora et al., 2019; Yun et al., 2021; Du et al., 2018; Li et al., 2021; Min et al., 2023; Chen et al., 2024a). Its landscape enjoys a favorable structure: the global minimum is attained and every stationary point is either a global minimizer or a strict saddle (Li et al., 2019b; Valavi et al., 2020; Zhou et al., 2022). Nevertheless, this problem retains a key complexity typical of neural network optimization: global minimizers can differ substantially (although they yield the same end-to-end matrix). In particular, in the unregularized case, both the parameter norm $\|U\|_F^2 + \|V\|_F^2$ and the imbalance $\|UU^\top - VV^\top\|_F^2$ can be arbitrarily large on the set of minimizers. This makes the problem a natural testbed for studying how hyperparameter choices affect the implicit biases of parameter optimization algorithms. We note that other forms of regularization have also been studied in the literature, such as $\|UU^\top - VV^\top\|_F^2$ (Tu et al., 2016; Ge et al., 2017).

We consider gradient descent with constant step size η to solve problem (1):

$$U_{t+1} = U_t - \eta V_t (V_t^\top U_t - Y^\top) - \eta\lambda U_t, \quad V_{t+1} = V_t - \eta U_t (U_t^\top V_t - Y) - \eta\lambda V_t.$$

We define the gradient descent update map $\mathrm{GD}_\eta(\theta) = \theta - \eta\nabla L(\theta)$ so that $(U_{t+1}, V_{t+1}) = \mathrm{GD}_\eta(U_t, V_t)$. The *basin of attraction* of a stationary point θ^* of L is the set of all initializations that converge to θ^*, $\{\theta\colon \lim_{N\to\infty} \mathrm{GD}_\eta^N(\theta) = \theta^*\}$ [1]. The *convergence region* for step size η, denoted by $\mathcal{D}_\eta$, is the union of the basins of attraction of all global minimizers. The *critical step size* $\eta(\bar{U}, \bar{V})$ for an initialization $(\bar{U}, \bar{V})$ is defined as $\eta(\bar{U}, \bar{V}) = \sup\{\eta\colon \lim_{N\to\infty} \mathrm{GD}_\eta^N(\theta) \in \mathcal{M}\}$, i.e., the supremum of the step sizes that allow convergence, where $\mathcal{M}$ denotes the set of all global minimizers.

We introduce notions for describing fractal geometry. A fractal is typically defined as a shape that exhibits self-similarity and fine structure at arbitrarily small scales. Formally, we say a set $S \subset \mathbb{R}^n$ is *self-similar with degree k* if there exist k homeomorphisms, $\phi_i\colon S \to S, i = 1, \cdots, k$, that satisfy (i) $S = \cup_{i=1}^k \phi_i(S)$ and (ii) there exists an open set $O \subset S$ such that $\cup_{i=1}^k \phi_i(O) \subset O$ and $(\phi_i(O))_{i=1}^k$ are pairwise disjoint. Condition (i) states that S can be covered by k smaller copies of itself. Condition (ii), which is known as the open set condition, ensures that those copies do not overlap much. This definition is closely related to an Iterated Function System (IFS), a standard tool for analyzing fractals (see, e.g., Hutchinson, 1981; Falconer, 2013). However, unlike IFS where the maps are required to be contractive and the set S to be compact, the shapes considered in our study may be unbounded.

Finally, we introduce notions related to chaos. Although there is no universal definition of chaos, one common characterization of chaos is the sensitivity to initialization, which is often known as the *butterfly effect*. In the context of optimization, this manifests as the phenomenon where infinitesimal perturbations of the parameter initialization or step size can lead to substantially different training outcomes (e.g., turning convergence into divergence, or shifting convergence from one minimizer to another qualitatively different minimizer). In dynamical systems, one of the most important measures of chaos is the *topological entropy*. Informally, the topological entropy $h(F)$ of a dynamical system F measures the exponential growth rate of the number of distinct trajectories of F as a function of the trajectory length. We defer the formal definition to Appendix B.1. A positive topological entropy is widely regarded as a hallmark of chaos (see, e.g., Katok et al., 1995; Robinson, 1998; Vries, 2014). In this paper, we adopt the above notions for fractals and chaos. We note that different definitions and settings exist, and discuss their relation to our study in Appendix A.

3 Simplified Matrix Factorization

In this section, we study gradient descent in the special case of problem (1) where $d_y = 1$, i.e., factorizing a scalar y as the inner product of two vectors as $u^\top v$. This and similar scalar factorization settings have served as canonical models for understanding large-step-size dynamics (Lewkowycz et al., 2020; Wang et al., 2022; Kreisler et al., 2023; Ahn et al., 2023; Zhu et al., 2023). Compared to these works, our analysis extends to critical step sizes, rather than restricting to bounded step sizes, and characterizes the chaos in gradient descent. Proofs for results in this section are in Appendix E.

[1] In dynamical systems the basin of attraction is often defined for attractors. Here we extend the terminology to include all stationary points, such as saddles, for simplicity of presentation.

3.1 CHAOS AT LARGE STEP SIZE

Consider the unregularized scalar factorization problem:

$$\min_{\theta=(u,v)\in\mathbb{R}^{2d}} \; L(\theta) = \frac{1}{2}(u^\top v - y)^2, \tag{2}$$

where $u, v \in \mathbb{R}^d$, $d \geq 1$ and $y \in \mathbb{R}$. Problem (2) retains several key complexities of the general problem (1), including non-convexity, high-dimensionality, non-Lipschitz gradients, and an unbounded set of global minimizers $\mathcal{M} = \{u^\top v = y\}$.

In the following result, we characterize the critical step size for problem (2) and the emergence of chaos under critical step sizes. We use $B(\theta, \varepsilon)$ to denote the ball of radius ε centered at θ.

Theorem 1 (Unregularized Scalar Factorization)**.** *Consider gradient descent with step size η for solving problem* (2)*. The following holds:*

- ***Critical Step Size:*** *For almost all initializations $(\bar{u}, \bar{v}) \in \mathbb{R}^{2d}$, the algorithm converges to a global minimizer if $\eta < \eta^*(\bar{u}, \bar{v})$ and fails to converge to any minimizer if $\eta > \eta^*(\bar{u}, \bar{v})$, where the critical step size is given by (when $y = 0$, we adopt the convention $1/0 = +\infty$):*

$$\eta^*(\bar{u}, \bar{v}) = \min\left\{\frac{1}{|y|}, \; \frac{8}{\|\bar{u}\|_2^2 + \|\bar{v}\|_2^2 + \sqrt{(\|\bar{u}\|_2^2 + \|\bar{v}\|_2^2)^2 - 16y(\bar{u}^\top\bar{v} - y)}}\right\}. \tag{3}$$

  Therefore, when η satisfies $\eta|y| < 1$, the convergence region $\mathcal{D}_\eta$ is equal almost everywhere to $\mathcal{D}'_\eta = \left\{(u, v) \in \mathbb{R}^{2d} \colon \|u\|_2^2 + \|v\|_2^2 + \sqrt{(\|u\|_2^2 + \|v\|_2^2)^2 - 16y(u^\top v - y)} < \frac{8}{\eta}\right\}$.

- ***Sensitivity to Initialization:*** *Fix a step size η that satisfies $\eta|y| < 1$. Let $\gamma_{\min} = \min\{\|\theta\| \colon \theta \in \mathcal{M}\}$ be the minimal norm over all global minimizers. Given arbitrary $\theta \in \partial\mathcal{D}'_\eta$, $\varepsilon, K > 0$ and $\gamma \in [\gamma_{\min}, \infty)$, there exist $\theta', \theta'', \theta''' \in B(\theta, \varepsilon)$ such that, as N tends to infinity, $\mathrm{GD}_\eta^N(\theta')$ converges to a global minimizer with norm γ, $\mathrm{GD}_\eta^N(\theta'')$ converges to a global minimizer with $\|uu^\top - vv^\top\|_F > K$, and $\mathrm{GD}_\eta^N(\theta''')$ converges to $(\mathbf{0}, \mathbf{0})$, which is a saddle when $y \neq 0$.*

- ***Trajectory Complexity:*** *Assume $\eta|y| < 1$. The topological entropy of the gradient descent system GD_η satisfies $h(\mathrm{GD}_\eta) \geq \log 3$. Moreover, GD_η has periodic orbits of any positive integer period.*

Theorem 1 provides a tight convergence condition for gradient descent in problem (2). The critical step size (3) consists of two components: The first term comes from the fact that, when $\eta|y| > 1$, all global minimizers become unstable and only attract a measure-zero set. The second term is associated with the convergence region. Notice that the critical step size depends smoothly on the initialization and that for $\eta < 1/|y|$ the convergence region is equal almost everywhere to an ellipsoid $\mathcal{D}'_\eta$ in $\mathbb{R}^{2d}$ (see right panel of Figure 1). This result improves the sufficient condition for convergence obtained by Wang et al. (2022), $\eta < \eta_1^*(\bar{u}, \bar{v}) = \min\left\{\frac{1}{3|y|}, \frac{4}{\|\bar{u}\|^2 + \|\bar{v}\|^2 + 4|y|}\right\}$. For $y \neq 0$, their threshold η_1^* is strictly smaller than the critical step size η^* in (3).

Theorem 1 provides a precise description of chaos in gradient descent: it has sensitive dependence on the initialization. Note that in problem (2), the squared norm of the parameter coincides with the loss sharpness $\lambda_{\max}(\nabla^2 L)$ at global minimizers (see Appendix E.1.2). Hence, Theorem 1 shows that at critical step size, infinitesimal perturbations of the initialization can send the trajectory to a minimizer with arbitrarily large norm, sharpness or imbalance, or to a saddle. This is a hallmark of unpredictability: it is impossible to reduce the error in the prediction of the converging point by improving the precision in the specification of the initialization. We remark that this form of strong reachability from an arbitrarily small range of initial values is familiar in chaos theory, for examples, the Julia sets in complex system and the Wada basin boundaries in flows and systems defined by diffeomorphisms (see, e.g., Devaney and Eckmann, 1987; Nusse and Yorke, 1996; Aguirre et al., 2001). However, these classical frameworks depend on properties not satisfied by our setting, for instance, complex differentiability or invertibility of the system map, and thus do not apply here.

Theorem 1 quantitatively measures chaos in gradient descent: the topological entropy is positive and is at least $\log 3$. This implies that, roughly, the number of distinct gradient descent trajectories

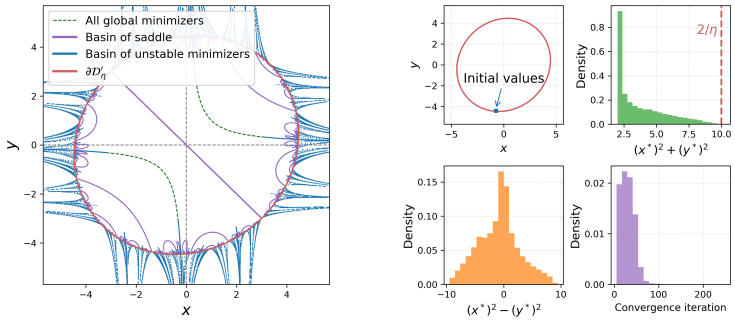

Figure 2: Left: Gradient descent applied to $L(x, y) = (xy - 1)^2$ with $(x, y) \in \mathbb{R}^2$. Blue lines and purple lines represent the basins of attraction of unstable minimizers and of the saddle $(\mathbf{0}, \mathbf{0})$, respectively. Right: For the same problem, we evenly sample initial values in an neighborhood on $\partial\mathcal{D}'_\eta$ (the blue square). We report the distributions of the squared norm and imbalance of the converged minimizer (x^*, y^*), and of the number of iterations to reach a loss below 10^{-8}.

of length N grows at a rate of 3^N (further interpretation for topological entropy is provided in Appendix B.1). Beyond entropy, another aspect of trajectory complexity is shown: gradient descent admits periodic orbits of any positive integer period. This property is closely related to Li-Yorke chaos and was shown for gradient descent in univariate loss functions (Kong and Tao, 2020; Chen et al., 2024b). Note, the parameter space of problem (2) has dimension $2d$ with $d \geq 1$.

While Theorem 1 identifies the convergence region up to a measure-zero set, we now provide a complete description of the region. In Appendix E.1.1, we showed that every minimizer with squared norm larger than $2/\eta$ is Lyapunov-unstable and that, the basins of attraction of unstable minimizers and of the saddle have measure zero. Note, by Theorem 1, these measure-zero basins intersect $\partial\mathcal{D}'_\eta$ in arbitrarily small neighborhoods and exhibit fractal structure (see left panel of Figure 2). The full convergence region $\mathcal{D}_\eta$ is then the union of the smooth domain $\mathcal{D}'_\eta$ and the basins of unstable minimizers, excluding the basin of with the saddle $(\mathbf{0}, \mathbf{0})$ when $y \neq 0$. We remark that, due to their zero measure, the basins of unstable minimizers and of the saddle cannot be easily detected by simulating training and were not been identified in prior work (Zhu et al., 2023). We visualize them with specialized techniques, with details provided in Appendix H.

Additional experiments are conducted for the distributional behavior of gradient descent. In the right panel of Figure 2, we evenly sampled 400^2 initial values in a small neighborhood on $\partial\mathcal{D}'_\eta$ and ran gradient descent for problem (2). For initial values that converge, we report the distribution of the squared norm and imbalancedness of the converged minimizers, as well as the number of iterations for convergence (reaching a preset convergence criterion). Notice that as predicted the norms are bounded by $2/\eta$. Notably, even though the initial values are drawn from a very small neighborhood, the distributions have wide supports. This implies sensitivity to initialization not only at the point level but also *at the distribution level*. Meanwhile, the distributions are not uniform, which means that gradient descent exhibits a form of distributional implicit bias under large step sizes. We leave a closer investigation of this interesting phenomenon to future work.

3.2 Regularization Induces Fractal Convergence Boundary

Consider the scalar factorization problem with ℓ_2 regularization:

$$\min_{\theta=(u,v)\in\mathbb{R}^{2d}} L(\theta) = \frac{1}{2}(u^\top v - y)^2 + \frac{\lambda}{2}(\|u\|_2^2 + \|v\|_2^2), \tag{4}$$

where $u, v \in \mathbb{R}^d$, $d \geq 1$, $\lambda \geq 0$ and $y \in \mathbb{R}$. The added regularization makes the set of global minimizers a bounded set. In particular, for problem (4), $\mathcal{M} = \{u = \text{sgn}(y)v, \|u\|_2^2 = |y| - \lambda\}$ when $\lambda < |y|$ and $\mathcal{M} = \{(\mathbf{0}, \mathbf{0})\}$ when $\lambda \geq |y|$. Regularization is commonly used to mitigate unbounded minimizers and to establish convergence results (Cabral et al., 2013; Ge et al., 2017; Li et al., 2019a). However, and rather remarkably, we will show that for the regularized problem the global dynamics of gradient descent becomes even more unpredictable than for the unregularized problem: not only is the limiting point of convergent trajectories unpredictable but also the convergence itself.

The predictability of convergence depends on the geometry of the boundary of the convergence region. Two difficulties arise in analyzing this geometry: (i) the presence of basin of the saddle; and (ii) the high-dimensionality of the convergence boundary. Specifically, we observe that the basin of attraction of the saddle point intricately penetrates $\mathcal{D}_\eta$ and creates topological boundaries "within" $\mathcal{D}_\eta$ (see Figure 4). However, such boundaries are not of interest, since they do not separate points inside $\mathcal{D}_\eta$ from those outside, i.e., both sides of boundary lie in $\mathcal{D}_\eta$. This motivates us to instead consider the boundary of $\mathcal{D}''_\eta = \mathcal{D}_\eta \cup \mathcal{S}_\eta$, where $\mathcal{S}_\eta$ is the basin of the saddle. Note, the smooth domain $\mathcal{D}'_\eta$ in the unregularized problem plays an analogous role in clarifying the geometry of convergence region.

The second difficulty is the high dimensionality of the boundary $\partial\mathcal{D}''_\eta \subset \mathbb{R}^{2d}$. To address this, we identify and reduce the symmetry in $\partial\mathcal{D}''_\eta$. We introduce the map $T\colon \mathbb{R}^{2d} \to \mathbb{R}^2$, $T(u, v) = (u^\top v, \|u\|_2^2 + \|v\|_2^2)$. The fiber of T, i.e., the preimage of a point in $T(\mathbb{R}^{2d})$, generically form a manifold diffeomorphic to $\mathbb{S}^{d-1} \times \mathbb{S}^{d-1}$ and hence have a regular shape (see Appendix D). In the following, we show that gradient descent dynamics are captured by their evolution across the fibers.

Proposition 2. *Let $(u_t, v_t)_{t\geq 0}$ denote the gradient descent trajectory in problem* (4) *with $\lambda \geq 0$. Let $(z_t, w_t) = T(u_t, v_t)$. There exists a planar map $F\colon \mathbb{R}^2 \to \mathbb{R}^2$ that only depends on η, λ, y such that $(z_{t+1}, w_{t+1}) = F(z_t, w_t)$ holds for all $t \geq 0$. In particular, (u_t, v_t) converges to $\mathcal{M}$ if and only if (z_t, w_t) converges to $\{z = y\}$, and it converges to $(\mathbf{0}, \mathbf{0})$ if and only if (z_t, w_t) converges to $(0, 0)$.*

The map F describes how the gradient descent trajectory evolves across the fibers of T. Its formulation is given in Appendix D. By Proposition 2, all points lying in the same fiber share the same convergence behavior. Therefore, roughly, the boundary $\partial\mathcal{D}''_\eta$ can be constructed by attaching fibers of T to the the projected boundary $T(\partial\mathcal{D}''_\eta)$; an example will be given below. Note, as the fibers are generically smooth manifolds, any geometric complexity of $\partial\mathcal{D}''_\eta$ will be captured by $T(\partial D''_\eta)$.

In the following result, we show that the convergence boundary of problem (4) has a self-similar structure and gradient descent exhibits sensitivity to initialization near the convergence boundary.

Theorem 3 (Regularized Scalar Factorization)**.** *Consider gradient descent with step size η for problem* (4) *with $0 < \lambda \leq \min\{(1/\eta) - |y|, 1/(2\eta)\}$. Consider the map $T(u, v) = (u^\top v, \|u\|_2^2 + \|v\|_2^2)$. Let $\mathcal{S}_\eta$ be the basin of attraction of $(\mathbf{0}, \mathbf{0})$, which is a saddle if $\lambda < |y|$, and let $\mathcal{D}''_\eta = \mathcal{D}_\eta \cup \mathcal{S}_\eta$.*

- ***Self-similarity:*** *$\mathcal{S}_\eta$ has measure zero and $T(\partial\mathcal{D}''_\eta)$ is self-similar with degree three.*
- ***Unboundedness****: When $y = 0$, there exist constants $a, b > 0$ such that almost all initializations $(\bar{u}, \bar{v})$ with $|\bar{u}^\top \bar{v}| < a\exp(-b(\|\bar{u}\|_2^2 + \|\bar{v}\|_2^2))$ converge to a global minimizer.*
- ***Sensitivity to Initialization****: For any $\theta \in \mathcal{D}_\eta$, the algorithm converges either to the closest global minimizer $p^-(\theta) = \arg\min_{p\in\mathcal{M}} \|p - \theta\|^2$, or the farthest $p^+(\theta) = \arg\max_{p\in\mathcal{M}} \|p - \theta\|^2$ ($p^+(\theta) \neq p^-(\theta)$ when $\lambda < |y|$). Moreover, there exist infinitely many points on $\partial\mathcal{D}''_\eta$ such that for any open set O containing such a point, there exist $\theta', \theta'' \in O$ such that $\mathrm{GD}^N(\theta')$ converges to $p^-(\theta')$ and $\mathrm{GD}^N(\theta'')$ converges to $p^+(\theta'')$, as N tends to infinity.*

Theorem 3 characterizes the geometry of the convergence boundary for problem (4). Specifically, $\partial\mathcal{D}''_\eta$ can be understood as a fiber-bundle-like object[2]: fibers of T, which are generically smooth and bounded manifolds, are attached to a self-similar set $T(\partial\mathcal{D}''_\eta)$ with degree three (see the left panel of Figure 3). The case of $d = 1$, i.e., $u, v \in \mathbb{R}$, is illustrated in the middle panel of Figure 3: in this case, the fibers are generically a four-point set and hence, $\partial\mathcal{D}''_\eta$ simply consists of four copies of $T(\partial\mathcal{D}''_\eta)$. To quantify the fractality, we estimate the box-counting dimension of $T(\partial\mathcal{D}''_\eta)$, which turns out to be 1.249 (see the right panel of Figure 3). This non-integer dimension implies that $T(\partial\mathcal{D}''_\eta)$ is essentially more complex than any smooth curve, yet fails to occupy any planar area. The fractal boundary marks unpredictability in convergence: when the initial point lies near the boundary, it is practically impossible to determine whether it is inside or outside the convergence region. This unpredictability is also quantified by the box-counting dimension, as explained in Appendix B.2.

Theorem 3 shows that, up to a measure-zero set, the convergence region has an unbounded interior. This sharply contrasts with the convergence region in the unregularized case, which coincides almost everywhere with a bounded domain. By Theorem 3, gradient descent converges provided that the $u^\top v$

[2]It is not a rigorous fiber bundle since the fiber $T^{-1}(z, w)$ might degenerate when (z, w) is a singular value.

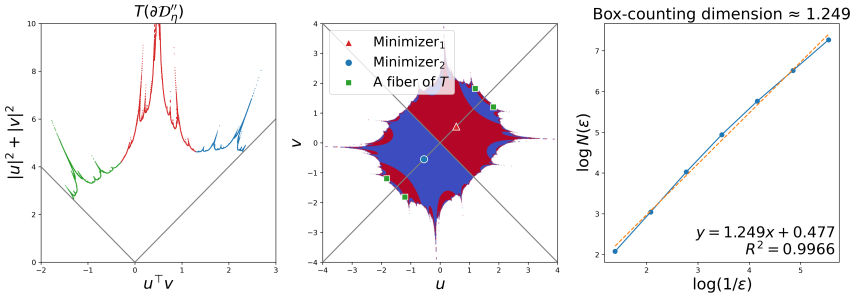

Figure 3: Gradient descent is applied to $L(u, v) = (uv - 0.5)^2/2 + 0.1(u^2 + v^2)$ where $(u, v) \in \mathbb{R}^2$. Left: the projected convergence boundary $T(\partial\mathcal{D}''_\eta)$ is self-similar with degree three: it is covered by three smaller copies of itself (green, red, blue). Middle: The convergence boundary $\partial\mathcal{D}''_\eta$ consists of four replicates of $T(\partial\mathcal{D}''_\eta)$, separated by gray lines. The only two minimizers are shown as red triangle and blue circle. Points are colored red if they converge to the red triangle, and blue if they converge to the blue circle. Right: the box-counting dimension of $T(\partial\mathcal{D}_\eta)$ is estimated as 1.249.

decays exponentially fast as a function of the squared norm $\|u\|_2^2 + \|v\|_2^2$. Geometrically, this creates an outward spike in the convergence region. Then, the self-similarity replicates this spike infinitely many times and at multiple scales, giving rise to the spiky convergence boundary observed in Figure 3. Although Theorem 3 shows the unboundedness only for the case $y = 0$, we observe qualitatively the same convergence region for general targets (for an example, see left panel in Figure 1).

Fractal basin boundaries have been extensively studied in dynamical systems (see, e.g., Grebogi et al., 1983b; McDonald et al., 1985). However, these classical approaches are either largely case-specific or rely on properties that do not hold in our settings, for instance, invertibility of the system map. A more detailed discussion is in Appendix A. To our knowledge, our result provides the first rigorous characterization of a fractal convergence region in the context of machine learning optimization.

Theorem 3 also shows that, although regularization eliminates unbounded global minimizers, the selected minimizer remains unpredictable. Specifically, the algorithm always selects either the minimal distance solution or the maximal distance solution over the set of global minimizers. However, this selection becomes unpredictable near the convergence boundary, as both choices can occur in arbitrarily small neighborhood (see middle panel of Figure 3). This stands is contrast with gradient descent under small step sizes, which typically is biased to the minimal distance solution (see, e.g., Gunasekar et al., 2018; Boursier et al., 2022). In fact, in Theorem 4 below, we show that this bias appears when the step size is small enough.

In the following result, we show that both the convergence and the converged minimizer are predictable when step size is sufficiently small.

Theorem 4. *Under the same conditions and notations as Theorem 3 and letting* $Q(u, v) = \|u\|_2^2 + \|v\|_2^2 + \sqrt{(\|u\|_2^2 + \|v\|_2^2)^2 - 16y(u^\top v - y)}$*, the following holds for almost all initializations* $(\bar{u}, \bar{v})$*: If* $\eta < 8/(4\lambda + Q(\bar{u}, \bar{v}))$*, then gradient descent converges to a global minimizer; If* $\eta < 4/(4\lambda + Q(\bar{u}, \bar{v}))$*, then the particular minimizer it converges to is* $p^-(\bar{u}, \bar{v})$*.*

Finally, we present another implication of the chaos in gradient descent. In Appendix F, we show for the case $d = 1$, i.e., $L(u, v) = \frac{1}{2}(uv - y)^2 + \frac{\lambda}{2}(u^2 + v^2)$, $u, v \in \mathbb{R}, \lambda \geq 0$, that, any continuous *dynamical invariant* must be constant. In particular, the *imbalance* $u^2 - v^2$, which is known to be (approximately) preserved under gradient descent with small step sizes (Du et al., 2018; Arora et al., 2019), fails dramatically under large step sizes. Although this result does not directly extend to the case $d \geq 2$, we anticipate that the chaos strongly constrains the form of dynamical invariants.

4 General Matrix Factorization

We extend the results of Section 3 to matrix factorization (1). The key observation is that when the initialization lies in a particular slice $\mathcal{W} \subset \mathbb{R}^{2d \cdot d_y}$ of the parameter space, the trajectory stays in the slice and the dynamics decomposes into several parallel sub-dynamics in scalar factorization.

Proposition 5. *Consider gradient descent with step size η for problem* (1) *with $d \geq d_y$. Consider the set $\mathcal{W} = \big\{(U, V) \in \mathbb{R}^{2d \cdot d_y} : \ \langle u^i, u^j \rangle = \langle u^i, v^j \rangle = \langle v^i, v^j \rangle = 0, \ \forall i \neq j\big\}$, where u^i, v^i denote the ith column of matrices U, V. The set $\mathcal{W}$ is forward-invariant, i.e., $\mathrm{GD}_\eta(\mathcal{W}) \subset \mathcal{W}$. Moreover, if the initialization $(\bar{U}, \bar{V}) \in \mathcal{W}$, then for $i = 1, \cdots, r$, the trajectory of the columns (u^i, v^i) is identical to the trajectory of gradient descent applied to scalar factorization problem $L_i(u, v) = \frac{1}{2}(u^\top v - y_i)^2 + \frac{\lambda}{2}(\|u\|_2^2 + \|v\|_2^2)$, with step size η and initialization $(\bar{u}^i, \bar{v}^i)$.*

With this observation, all results presented in Section 3 extend verbatim to problem (1) with initializations in $\mathcal{W}$. We present the detailed extensions in Appendix G. Note, the slice $\mathcal{W}$ contains non-trivial, i.e., non-zero, initializations if and only if $d \geq d_y$. Thus, our results do not cover the low-rank setting. However, $\mathcal{W}$ contains the identity initializations $\bar{U} = \alpha I_d, \bar{V} = \beta I_d$ for $d = d_y$, and the zero-asymmetric initialization (Wu et al., 2019). The identity initialization is common in training deep linear networks (Chou et al., 2024; Ghosh et al., 2025) and is closely related the training of linear residual networks (Hardt and Ma, 2017; Bartlett et al., 2018). Our results therefore also apply in those setting. Although our results are established for initializations in $\mathcal{W}$, we experimentally verify that the chaotic phenomena persist over general initializations and in deep matrix factorization; details are provided in Appendix G.

Discussion of the mechanism We provide an intuitive explanation for the emergence of chaos in matrix factorization. Although the update map GD_η is non-invertible, in Appendix G we show that the parameter space is partitioned by a measure-zero set $\mathcal{K}_\eta$, so that the restriction of GD_η to each connected component of $\mathbb{R}^{2d \cdot d_r} \setminus \mathcal{K}_\eta$ is a covering map. This measure-zero set comprises primarily the critical points of the map GD_η, $\big\{\theta \in \mathbb{R}^{2d \cdot d_y} : \ \det J(\mathrm{GD}_\eta(\theta)) = \det(I - \eta \nabla^2 L(\theta)) = 0\big\}$, which are the points where the Hessian of the loss has an eigenvalue equal to $1/\eta$. We reason that chaotic phenomena arise when there exists a connected component $\mathcal{C} \subset \mathbb{R}^{2d \cdot d_y} \setminus \mathcal{K}_\eta$ that satisfies (i) $\mathcal{C}$ contains at least two global minimizers, and (ii) $\mathcal{C} \subseteq \mathrm{GD}_\eta(\mathcal{C})$. To see this, assume that GD_η has covering degree m. For any minimizer $p \in \mathcal{C}$, since $p \in \mathcal{C} \subseteq \mathrm{GD}_\eta(\mathcal{C})$, there exists a neighborhood O_p of p such that $\mathrm{GD}^{-1}(O_p)$ has m connected components that are contained in $\mathcal{C}$. By induction, the preimage of O_p under the Nth iteration map, $\mathrm{GD}^{-N}(O_p)$, has m^N components. Then the basin of attraction of points near p is $B(p) = \cup_{N=1}^{\infty} \mathrm{GD}^{-N}(O_p)$, which has infinitely many components. These accumulate at the convergence boundary, as the boundary often contains an invariant set with expanding directions and thus attracts inverse dynamics. Since the same phenomenon holds for all global minimizers in $\mathcal{C}$, their associated basins tend to be intricately interwoven near the convergence boundary, which gives rise to sensitive dependence on the initialization (see right panel of Figure 1). Additionally, by definition, $B(p) = \mathrm{GD}_\eta(B(p))$, which means that $B(p)$ can be folded m times onto itself. This characterizes a self-similar structure. We point out that although this heuristic provides an intuitive explanation for the emergence of chaos, a rigorous investigation is left for future work.

5 Conclusion

We offered a rigorous characterization of gradient descent with large step sizes in matrix factorization. Our results reveal two striking phenomena: near the convergence boundary, the selection of the minimizer is unpredictable, and adding regularization can induce a fractal convergence boundary that makes the convergence itself unpredictable. As a driver of this complexity, we suggested a covering map structure exhibited by the gradient update map on parameter regions where the inverse step size is not an eigenvalue of the Hessian of the loss.

Limitations Although our characterizations substantially expand the state of knowledge in non-convex overparametrized optimization in the particular setting of matrix factorization, further research is needed to rigorously characterize the dynamics of large-step-size gradient descent in other settings, such as general initializations, deep matrix factorization, or neural networks with nonlinear activation functions. We believe the contributed insights can aid in the development of such program.

Future directions We showed that at large step sizes there may not exist any simple algorithmic biases, but observed that biases could still be studied in a distribution sense. Further analyzing the properties of the distribution over global minimizers that is induced by a distribution of initializations is an interesting direction for future work. In particular, are there cases in which the distribution is uniform over a subset of minimizers, or cases in which it will concentrate in a predictable way?

Reproducibility statement Code to reproduce our experiments is made available at `https://anonymous.4open.science/r/chaos-matrix-factorization-07C5`.

REFERENCES

Agarwala, A., Pedregosa, F., and Pennington, J. (2023). Second-order regression models exhibit progressive sharpening to the edge of stability. In *Proceedings of the 40th International Conference on Machine Learning*, pages 169–195.

Aguirre, J., Vallejo, J. C., and Sanjuán, M. A. (2001). Wada basins and chaotic invariant sets in the hénon-heiles system. *Physical Review E*, 64(6):066208.

Aguirre, J., Viana, R. L., and Sanjuán, M. A. (2009). Fractal structures in nonlinear dynamics. *Reviews of Modern Physics*, 81(1):333–386.

Ahn, K., Bubeck, S., Chewi, S., Lee, Y. T., Suarez, F., and Zhang, Y. (2023). Learning threshold neurons via edge of stability. *Advances in Neural Information Processing Systems*, 36:19540–19569.

Ahn, K., Zhang, J., and Sra, S. (2022). Understanding the unstable convergence of gradient descent. In *International conference on machine learning*, pages 247–257. PMLR.

Andriushchenko, M., Varre, A. V., Pillaud-Vivien, L., and Flammarion, N. (2023). SGD with large step sizes learns sparse features. In *International Conference on Machine Learning*, pages 903–925. PMLR.

Arora, S., Cohen, N., Golowich, N., and Hu, W. (2019). A convergence analysis of gradient descent for deep linear neural networks. In *International Conference on Learning Representations*.

Ba, J., Erdogdu, M. A., Suzuki, T., Wang, Z., Wu, D., and Yang, G. (2022). High-dimensional asymptotics of feature learning: How one gradient step improves the representation. In *Advances in Neural Information Processing Systems*.

Bartlett, P., Helmbold, D., and Long, P. (2018). Gradient descent with identity initialization efficiently learns positive definite linear transformations by deep residual networks. In *International conference on machine learning*, pages 521–530. PMLR.

Boursier, E., Pillaud-Vivien, L., and Flammarion, N. (2022). Gradient flow dynamics of shallow ReLU networks for square loss and orthogonal inputs. In *Advances in Neural Information Processing Systems*, volume 35, pages 20105–20118. Curran Associates, Inc.

Bowen, R., Ruelle, D., and Chazottes, J. (2008). *Equilibrium States and the Ergodic Theory of Anosov Diffeomorphisms*. Lecture Notes in Mathematics. Springer Berlin Heidelberg.

Cabral, R., De la Torre, F., Costeira, J. P., and Bernardino, A. (2013). Unifying nuclear norm and bilinear factorization approaches for low-rank matrix decomposition. In *Proceedings of the IEEE international conference on computer vision*, pages 2488–2495.

Cai, Y., Wu, J., Mei, S., Lindsey, M., and Bartlett, P. (2024). Large stepsize gradient descent for non-homogeneous two-layer networks: Margin improvement and fast optimization. *Advances in Neural Information Processing Systems*, 37:71306–71351.

Chen, H., Chen, X., Elmasri, M., and Sun, Q. (2024a). Gradient descent in matrix factorization: Understanding large initialization. In *Uncertainty in Artificial Intelligence*, pages 619–647. PMLR.

Chen, L. and Bruna, J. (2023). Beyond the edge of stability via two-step gradient updates. In *International Conference on Machine Learning*, pages 4330–4391. PMLR.

Chen, P., Jiang, R., and Wang, P. (2025). A complete loss landscape analysis of regularized deep matrix factorization. *arXiv preprint arXiv:2506.20344*.

Chen, X., Balasubramanian, K., Ghosal, P., and Agrawalla, B. K. (2024b). From stability to chaos: Analyzing gradient descent dynamics in quadratic regression. *Transactions on Machine Learning Research*.

Chou, H.-H., Gieshoff, C., Maly, J., and Rauhut, H. (2024). Gradient descent for deep matrix factorization: Dynamics and implicit bias towards low rank. *Applied and Computational Harmonic Analysis*, 68:101595.

Cohen, J., Kaur, S., Li, Y., Kolter, J. Z., and Talwalkar, A. (2021). Gradient descent on neural networks typically occurs at the edge of stability. In *International Conference on Learning Representations*.

Crăciun, A. and Ghoshdastidar, D. (2024). On the convergence of gradient descent for large learning rates. *arXiv preprint arXiv:2402.13108*.

Damian, A., Nichani, E., and Lee, J. D. (2023). Self-stabilization: The implicit bias of gradient descent at the edge of stability. In *The Eleventh International Conference on Learning Representations*.

Dandi, Y., Krzakala, F., Loureiro, B., Pesce, L., and Stephan, L. (2024). How two-layer neural networks learn, one (giant) step at a time. *Journal of Machine Learning Research*, 25(349):1–65.

Danovski, K., Soriano, M. C., and Lacasa, L. (2024). Dynamical stability and chaos in artificial neural network trajectories along training. *Frontiers in Complex Systems*, 2:1367957.

De Melo, W. and Van Strien, S. (2012). *One-dimensional dynamics*, volume 25. Springer Science & Business Media.

Devaney, R. L. and Eckmann, J.-P. (1987). An introduction to chaotic dynamical systems.

Du, S. S., Hu, W., and Lee, J. D. (2018). Algorithmic regularization in learning deep homogeneous models: Layers are automatically balanced. *Advances in neural information processing systems*, 31.

Elaydi, S. N. (2007). *Discrete chaos: with applications in science and engineering*. Chapman and Hall/CRC.

Falconer, K. (2013). *Fractal geometry: mathematical foundations and applications*. John Wiley & Sons.

Ge, R., Jin, C., and Zheng, Y. (2017). No spurious local minima in nonconvex low rank problems: A unified geometric analysis. In *International conference on machine learning*, pages 1233–1242. PMLR.

Ghosh, A., Kwon, S. M., Wang, R., Ravishankar, S., and Qu, Q. (2025). Learning dynamics of deep matrix factorization beyond the edge of stability. In *The Second Conference on Parsimony and Learning (Recent Spotlight Track)*.

Golubitsky, M. and Stewart, I. (2003). *The symmetry perspective: from equilibrium to chaos in phase space and physical space*, volume 200. Springer Science & Business Media.

Grebogi, C., McDonald, S. W., Ott, E., and Yorke, J. A. (1983a). Final state sensitivity: an obstruction to predictability. *Physics Letters A*, 99(9):415–418.

Grebogi, C., Ott, E., and Yorke, J. A. (1983b). Fractal basin boundaries, long-lived chaotic transients, and unstable-unstable pair bifurcation. *Physical Review Letters*, 50(13):935.

Gunasekar, S., Lee, J., Soudry, D., and Srebro, N. (2018). Characterizing implicit bias in terms of optimization geometry. In *Proceedings of the 35th International Conference on Machine Learning*, volume 80, pages 1832–1841. PMLR.

Hardt, M. and Ma, T. (2017). Identity matters in deep learning. In *International Conference on Learning Representations*.

Herrmann, L., Granz, M., and Landgraf, T. (2022). Chaotic dynamics are intrinsic to neural network training with sgd. *Advances in Neural Information Processing Systems*, 35:5219–5229.

Hunt, B. R., Ott, E., and Rosa Jr, E. (1999). Sporadically fractal basin boundaries of chaotic systems. *Physical review letters*, 82(18):3597.

Hutchinson, J. E. (1981). Fractals and self similarity. *Indiana University Mathematics Journal*, 30(5):713–747.

Jastrzebski, S., Szymczak, M., Fort, S., Arpit, D., Tabor, J., Cho, K., and Geras, K. (2020). The break-even point on optimization trajectories of deep neural networks. In *International Conference on Learning Representations*.

Jelonek, Z. (2002). Geometry of real polynomial mappings. *Mathematische Zeitschrift*, 239(2):321–333.

Jiménez-González, P., Soriano, M. C., and Lacasa, L. (2025). Leveraging chaos in the training of artificial neural networks. *arXiv preprint arXiv:2506.08523*.

Kalra, D. S. and Barkeshli, M. (2023). Phase diagram of early training dynamics in deep neural networks: effect of the learning rate, depth, and width. *Advances in Neural Information Processing Systems*, 36:51621–51662.

Katok, A., Katok, A., and Hasselblatt, B. (1995). *Introduction to the modern theory of dynamical systems*. Cambridge university press.

Kong, L. and Tao, M. (2020). Stochasticity of deterministic gradient descent: Large learning rate for multiscale objective function. *Advances in neural information processing systems*, 33:2625–2638.

Kreisler, I., Nacson, M. S., Soudry, D., and Carmon, Y. (2023). Gradient descent monotonically decreases the sharpness of gradient flow solutions in scalar networks and beyond. In *International Conference on Machine Learning*, pages 17684–17744. PMLR.

Lee, J. (2000). *Introduction to topological manifolds*. Springer.

Lee, J. (2012). *Introduction to Smooth Manifolds*. Graduate Texts in Mathematics. Springer New York.

Lewkowycz, A., Bahri, Y., Dyer, E., Sohl-Dickstein, J., and Gur-Ari, G. (2020). The large learning rate phase of deep learning: the catapult mechanism. *arXiv preprint arXiv:2003.02218*.

Li, Q., Zhu, Z., and Tang, G. (2019a). The non-convex geometry of low-rank matrix optimization. *Information and Inference: A Journal of the IMA*, 8(1):51–96.

Li, T.-Y. and Yorke, J. A. (1975). Period three implies chaos. *The American Mathematical Monthly*, 82(10):985–992.

Li, X., Lu, J., Arora, R., Haupt, J., Liu, H., Wang, Z., and Zhao, T. (2019b). Symmetry, saddle points, and global optimization landscape of nonconvex matrix factorization. *IEEE Transactions on Information Theory*, 65(6):3489–3514.

Li, Z., Luo, Y., and Lyu, K. (2021). Towards resolving the implicit bias of gradient descent for matrix factorization: Greedy low-rank learning. In *International Conference on Learning Representations*.

Lu, M., Wu, B., Yang, X., and Zou, D. (2024). Benign oscillation of stochastic gradient descent with large learning rate. In *The Twelfth International Conference on Learning Representations*.

Ma, C., Wu, L., and Ying, L. (2022). The multiscale structure of neural network loss functions: The effect on optimization and origin. *arXiv preprint arXiv:2204.11326*, 14.

McDonald, S. W., Grebogi, C., Ott, E., and Yorke, J. A. (1985). Fractal basin boundaries. *Physica D: Nonlinear Phenomena*, 17(2):125–153.

Meltzer, D. and Liu, J. (2023). Catapult dynamics and phase transitions in quadratic nets. *arXiv preprint arXiv:2301.07737*.

Meng, S. Y., Orvieto, A., Cao, D. Y., and De Sa, C. (2024). Gradient descent on logistic regression with non-separable data and large step sizes. *arXiv preprint arXiv:2406.05033*.

Menon, G. (2024). The geometry of the deep linear network. *arXiv preprint arXiv:2411.09004*.

Min, H., Vidal, R., and Mallada, E. (2023). On the convergence of gradient flow on multi-layer linear models. In *International Conference on Machine Learning*, pages 24850–24887. PMLR.

Moniri, B., Lee, D., Hassani, H., and Dobriban, E. (2025). A theory of non-linear feature learning with one gradient step in two-layer neural networks.

Mulayoff, R. and Michaeli, T. (2020). Unique properties of flat minima in deep networks. In *International conference on machine learning*, pages 7108–7118. PMLR.

Nacson, M. S., Mulayoff, R., Ongie, G., Michaeli, T., and Soudry, D. (2023). The implicit bias of minima stability in multivariate shallow relu networks. In *ICLR*.

Nacson, M. S., Ravichandran, K., Srebro, N., and Soudry, D. (2022). Implicit bias of the step size in linear diagonal neural networks. In *International Conference on Machine Learning*, pages 16270–16295. PMLR.

Nar, K. and Sastry, S. (2018). Step size matters in deep learning. *Advances in Neural Information Processing Systems*, 31.

Nusse, H. E. and Yorke, J. A. (1996). Wada basin boundaries and basin cells. *Physica D: Nonlinear Phenomena*, 90(3):242–261.

Ponomarev, S. P. (1987). Submersions and preimages of sets of measure zero. *Siberian Mathematical Journal*, 28(1):153–163.

Qiao, D., Zhang, K., Singh, E., Soudry, D., and Wang, Y.-X. (2024). Stable minima cannot overfit in univariate relu networks: Generalization by large step sizes. *Advances in Neural Information Processing Systems*, 37:94163–94208.

Robinson, C. (1998). *Dynamical systems: stability, symbolic dynamics, and chaos*. CRC press.

Rosa Jr, E. and Ott, E. (1999). Mixed basin boundary structures of chaotic systems. *Physical Review E*, 59(1):343.

Sadrtdinov, I., Kodryan, M., Pokonechny, E., Lobacheva, E., and Vetrov, D. P. (2024). Where do large learning rates lead us? *Advances in Neural Information Processing Systems*, 37:58445–58479.

Saxe, A. M., McClelland, J. L., and Ganguli, S. (2013). Exact solutions to the nonlinear dynamics of learning in deep linear neural networks. *arXiv preprint arXiv:1312.6120*.

Smale, S. (1967). Differentiable dynamical systems. *Bulletin of the American Mathematical Society*, 73(6):747 – 817.

Sohl-Dickstein, J. (2024). The boundary of neural network trainability is fractal. *arXiv preprint arXiv:2402.06184*.

Song, M. and Yun, C. (2023). Trajectory alignment: Understanding the edge of stability phenomenon via bifurcation theory. In *Thirty-seventh Conference on Neural Information Processing Systems*.

Sonthalia, R., Murray, M., and Montufar, G. (2025). Low rank gradients and where to find them. In *High-dimensional Learning Dynamics 2025*.

Tél, T. (1990). Transient chaos. *Directions in chaos*, 3:149–211.

Tu, S., Boczar, R., Simchowitz, M., Soltanolkotabi, M., and Recht, B. (2016). Low-rank solutions of linear matrix equations via procrustes flow. In *International conference on machine learning*, pages 964–973. PMLR.

Valavi, H., Liu, S., and Ramadge, P. (2020). Revisiting the landscape of matrix factorization. In *Proceedings of the Twenty Third International Conference on Artificial Intelligence and Statistics*, volume 108 of *Proceedings of Machine Learning Research*, pages 1629–1638. PMLR.

Van Den Doel, K. and Ascher, U. (2012). The chaotic nature of faster gradient descent methods. *Journal of Scientific Computing*, 51(3):560–581.

Vries, J. (2014). *Topological dynamical systems: an introduction to the dynamics of continuous mappings*, volume 59. Walter De Gruyter.

Wang, Y., Chen, M., Zhao, T., and Tao, M. (2022). Large learning rate tames homogeneity: Convergence and balancing effect. In *International Conference on Learning Representations*.

Wang, Y., Xu, Z., Zhao, T., and Tao, M. (2023). Good regularity creates large learning rate implicit biases: edge of stability, balancing, and catapult. In *NeurIPS 2023 Workshop on Mathematics of Modern Machine Learning*.

Wu, J., Bartlett, P. L., Telgarsky, M., and Yu, B. (2024). Large stepsize gradient descent for logistic loss: Non-monotonicity of the loss improves optimization efficiency. In Agrawal, S. and Roth, A., editors, *Proceedings of Thirty Seventh Conference on Learning Theory*, volume 247 of *Proceedings of Machine Learning Research*, pages 5019–5073. PMLR.

Wu, L., Ma, C., et al. (2018). How SGD selects the global minima in over-parameterized learning: A dynamical stability perspective. *Advances in Neural Information Processing Systems*, 31.

Wu, L. and Su, W. J. (2023). The implicit regularization of dynamical stability in stochastic gradient descent. In *International Conference on Machine Learning*, pages 37656–37684. PMLR.

Wu, L., Wang, Q., and Ma, C. (2019). Global convergence of gradient descent for deep linear residual networks. *Advances in Neural Information Processing Systems*, 32.

Xu, Z., Min, H., Tarmoun, S., Mallada, E., and Vidal, R. (2023). Linear convergence of gradient descent for finite width over-parametrized linear networks with general initialization. In *International Conference on Artificial Intelligence and Statistics*, pages 2262–2284. PMLR.

Ye, T. and Du, S. S. (2021). Global convergence of gradient descent for asymmetric low-rank matrix factorization. *Advances in Neural Information Processing Systems*, 34:1429–1439.

Yun, C., Krishnan, S., and Mobahi, H. (2021). A unifying view on implicit bias in training linear neural networks. In *International Conference on Learning Representations*.

Zhou, J., Li, X., Ding, T., You, C., Qu, Q., and Zhu, Z. (2022). On the optimization landscape of neural collapse under MSE loss: Global optimality with unconstrained features. In *International Conference on Machine Learning*, pages 27179–27202. PMLR.

Zhu, L., Liu, C., Radhakrishnan, A., and Belkin, M. (2024a). Catapults in sgd: spikes in the training loss and their impact on generalization through feature learning. In *International Conference on Machine Learning*, pages 62476–62509. PMLR.

Zhu, L., Liu, C., Radhakrishnan, A., and Belkin, M. (2024b). Quadratic models for understanding catapult dynamics of neural networks. In *The Twelfth International Conference on Learning Representations*.

Zhu, X., Wang, Z., Wang, X., Zhou, M., and Ge, R. (2023). Understanding edge-of-stability training dynamics with a minimalist example. In *International Conference on Learning Representations*.

Ziyin, L., Li, B., Simon, J. B., and Ueda, M. (2022). SGD can converge to local maxima. In *International Conference on Learning Representations*.

APPENDIX

The appendix is organized into the following sections.

- Appendix A: Relation to classical theory for chaos and fractals
- Appendix B: Measure of chaos in dynamical systems
- Appendix C: Diagonality of the target matrix
- Appendix D: Quotient dynamics of gradient descent
- Appendix E: Proofs for Section 3
- Appendix F: Non-existence of continuous dynamical invariant
- Appendix G: General matrix factorization
- Appendix H: Experiment details
- Appendix I: Additional experiments

A RELATION TO CLASSICAL THEORY FOR CHAOS AND FRACTALS

A.1 CHAOTIC DYNAMICAL SYSTEMS

A common definition of chaotic dynamical systems is by Devaney and Eckmann (1987). A dynamical system $F\colon X \to X$, where X is the state space, is chaotic if: (i) it is sensitive to initialization, (ii) it is topological transitive, and (iii) periodic points are dense in X. Here, sensitivity to initialization requires that there exists $\delta > 0$ such that for any $x \in X$ and any neighborhood of x, there exists $N > 0$ and y in the neighborhood such that $\mathrm{dist}(F^N(x), F^N(y)) > \delta$. This is weaker than the property we presented in Theorem 1 and Theorem 3: when the converged points of two trajectories are different, the trajectories must differ by a positive difference at some time N, but not vice versa. In Proposition 14, we show that the boundary $\partial\mathcal{D}'_\eta$, as defined in Theorem 1, is invariant under gradient descent. In Proposition 18, we show that when restricted to $\partial\mathcal{D}'_\eta$, the gradient descent system is semi-conjugate to a one-dimensional system that is precisely Devaney chaotic. However, we show in Proposition 19 that the original gradient descent system is not Devaney-chaotic when $d \geq 2$ as it fails to be topological transitive.

A system $F\colon X \to X$ is topological transitive if for any pair of non-empty open sets U, V, there exists N such that $F^N(U) \cap V \neq \varnothing$. A family of dynamical systems that exhibit transitivity is the family of *Axiom-A diffeomorphisms* (Smale, 1967). These are dynamical systems where the set of non-wandering points is hyperbolic and is equal to the closure of the set of periodic points. A closed set Λ is hyperbolic if it is forward invariant and at each point $x \in \Lambda$ the tangent space of the ambient space splits as a direct sum of stable and unstable subspaces. It is known that an Axiom-A diffeomorphism is always transitive on each of its *basic set* (Bowen et al., 2008, Chapter 3). However, gradient update maps typically are not expected to satisfy this definition as they in general are not global diffeomorphisms.

Another definition of chaotic dynamical system is by Li and Yorke (1975). They considered a dynamical system $F\colon X \to X$ with $X \subset \mathbb{R}$ being an interval chaotic if F has a periodic orbit with period three. They showed that if such a periodic orbit exists, then (i) F has periodic orbit with any period; (ii) there exists an uncountable set $S \subset J$ such that, for every $p, q \in S$ with $p \neq q$,

$$\limsup_{N\to\infty} |F^N(p) - F^N(q)| > 0, \ \liminf_{N\to\infty} |F^N(p) - F^N(q)| = 0,$$

and (iii) for every $p \in S$ and a periodic point $q \in J$,

$$\limsup_{N\to\infty} |F^N(p) - F^N(q)| > 0.$$

In Proposition 17, we showed that the restricted system $\mathrm{GD}_\eta|_{\partial\mathcal{D}'_\eta}$ is semi-conjugate to a one-dimensional system that is Li-Yorke chaotic. In general, Devaney chaos and Li-Yorke chaos do not imply each other. For a detailed comparison between different notions of chaotic dynamical systems, see Elaydi (2007).

A.2 FRACTAL BASIN BOUNDARY

The fractal convergence boundary studied in this work falls into a more general notion, called a fractal basin boundary. The seminal classification given by McDonald et al. (1985) divides fractal basin boundaries into three categories: quasicircles, locally connected but not quasicircles, and locally disconnected. The most regular type, quasicircle, is typical in the Julia sets of complex analytic maps. However, as noted by McDonald et al. (1985), properties of complex analytic maps do not generalize to real maps, and hence quasicircle is uncommon in real systems. We observe that the convergence boundary in our study falls in the second category, locally connected but not quasicircles. This type of boundary has been observed in several planar maps, i.e., dynamical systems defined on regions of $\mathbb{R}^2$. A well-known example is the following system:

$$x_{n+1} = \lambda_x x_n \mod (1), \quad y_{n+1} = \lambda_y y_n + \cos(2\pi x_n).$$

The basin boundary of this system is precisely the Weierstrass curve. McDonald et al. (1985) argued that a typical characteristic of this type of boundaries is the local stratification structure, which also appears in the convergence region in our case (see left panel in Figure 1). To our knowledge, however, all examples of locally connected boundaries appearing in the literature, including those presented by McDonald et al. (1985); Hunt et al. (1999); Rosa Jr and Ott (1999), are bounded, whereas the convergence region in our case is shown to be unbounded. Classical approaches do not apply to our study, as most of those theoretical studies are case-specific. The last category has the most complicated structure and, as noted by Aguirre et al. (2009), turns out to appear more commonly in physical systems. Boundaries in this category typically exhibit a Cantor set structure. Examples include the famous Hénon map and the horseshoe map. For a recent review of the fractal boundaries, we refer readers to Aguirre et al. (2009).

B MEASURE OF CHAOS IN DYNAMICAL SYSTEM

We introduce two measures of chaos in dynamical systems. In Appendix B.1 we introduce the topological entropy of a dynamical system and, in Appendix B.2 we discuss how the fractal dimension of the basin boundary implies unpredictability.

B.1 TOPOLOGICAL ENTROPY

Let $F\colon X \to X$ be a dynamical system, where X is the state space with a metric d. The idea behind topological entropy is to measure how fast the number of "distinct" trajectories increases as the trajectory length increases. To measure the difference between two trajectories of length N, consider

$$d_N(x, y) = \max_{0 \le i \le N-1} d(F^i(x), F^i(y)).$$

Then, the number of "distinct" trajectories of length N is measured by

$$r(N, \varepsilon) = \max\left\{|S|\colon\ d_N(x, y) > \varepsilon, \forall x, y \in S, x \neq y\right\},$$

where $|S|$ is the number of elements in S. The topological entropy of F, denoted $h(F)$, measures the exponential growth rate of $r(N, \varepsilon)$ as N increases. Specifically, $h(F)$ is defined as follows:

$$h(F) = \lim_{\varepsilon \to 0^+} \limsup_{N \to \infty} \frac{\log r(N, \varepsilon)}{N}.$$

We give an example to provide more intuition. Consider the following symbolic dynamical systems:

$$\sigma\colon\ \{0,1\}^\infty \to \{0,1\}^\infty,\ \sigma(s_0 s_1 s_2 \cdots) = (s_1 s_2 \cdots).$$

Here the state space $\{0,1\}^\infty$ denotes the set of all infinite sequence of two symbols 0 and 1, whose metric is defined by

$$d((s_0 s_1 \cdots), (s_0' s_1' \cdots)) = \sum_{j=0}^{\infty} \frac{|s_j - s_j'|}{2^j}.$$

The system σ is called the *full-shift on two symbols*. Despite its simple definition, this system is unpredictable and chaotic (see, e.g., Devaney and Eckmann, 1987). In particular, periodic points are dense in the state space, and, there exists a trajectory that is dense in the state space, i.e., there is a

single trajectory that can come arbitrarily close to any point. In terms of predictability, consider two points $\boldsymbol{s} = (s_0 s_1 \cdots), \boldsymbol{s}' = (s'_0 s'_1 \cdots)$ that have the same first m elements, but differ starting from the $(m+1)$th element. By the definition of the distance, we have $d(\boldsymbol{s}, \boldsymbol{s}') \leq \sum_{j=0}^{\infty} 1/2^{m+j} = 1/2^{m+1}$. However, for all $N \geq m$, we have $d(\sigma^N(\boldsymbol{s}), \sigma^N(\boldsymbol{s})) > 1/2$. Therefore, even if two initial points are arbitrarily close to each other, one can not make any prediction on how close their trajectories will remain in the long term. This unpredictability stems form the richness of "distinct" trajectories. In fact, one can show that $h(\sigma) = \log 2 > 0$ (see, e.g., Vries, 2014). Note, the topological entropy of the gradient descent in matrix factorization is at least $\log 3$ (Theorem 1).

B.2 Box-counting dimension and unpredictability

There have been numerous investigations discussing how a non-integer fractal dimension implies unpredictability in dynamical systems (see, e.g., Tél, 1990; Aguirre et al., 2009). Here we provide a brief introduction to this topic.

Recall that the *box-counting dimension* of a set S is defined as the following limit if it exists:

$$D_B(S) = \lim_{\varepsilon \to 0} \frac{\log(N(\varepsilon))}{\log(1/\varepsilon)},$$

where $N(\varepsilon)$ is the number of boxes of side length ε needed to cover the set S. For a dynamical system $F\colon X \to X$ where $X \subset \mathbb{R}^D$ is the state space, let D_B be the box-counting dimension of a basin boundary and D be the topology dimension of the state space. Consider a collection of trajectories and randomly perturb their initial points by a scale ε. Let $f(\varepsilon)$ denote the fraction of the trajectories that converge to a different point, i.e., whose initial point lies in a different basin of attraction after the perturbation. Thus, $f(\varepsilon)$ can be roughly viewed as the chance of making an error in predicting the converged point when the precision in specifying the initial point is ε. In general, the following scaling relation holds (Grebogi et al., 1983a):

$$f(\varepsilon) \sim \varepsilon^{D - D_B},$$

where $D - D_B$ is known as the *uncertainty exponent*. When the boundary is smooth, we have $D_B = D - 1$ and thus $f(\varepsilon) \sim \varepsilon$, i.e., the accuracy of the prediction of the converged point is proportional to the precision on the initial point. In contrast, when the boundary has a non-integer dimension, we have $D - 1 < D_B < D$ and hence $D - D_B < 1$. This implies that a substantial increase in the precision in specifying the initial point leads to only a very small increase in the accuracy of the prediction. This marks sensitivity to initialization and unpredictability. Note, the box-counting dimension of the projected boundary $T(\partial \mathcal{D}''_\eta)$ is estimated as 1.249, yielding an uncertainty exponent $2 - 1.249 = 0.751$ (see Section 3.2).

C Diagonality of the target matrix

We show that in matrix factorization (1), one may assume without lose of generality that the target matrix is diagonal. This simplification is a standard technique that has been widely adopted in the literature.

Let $Y = P_Y \Sigma_Y Q_Y^\top$ be the singular value decomposition of Y, where $P_Y, Q_Y \in O(d_y)$ and $\Sigma_Y \in \mathbb{R}^{d_y \times d_y}$ is diagonal. Consider the change of coordinates $U = \tilde{U} P_Y^\top$ and $V = \tilde{V} Q_Y^\top$. Recall that the U-update in minimizing $L(U, V)$ is given by

$$U_{t+1} = U_t - \eta V_t (V_t^\top U_t - Y^\top) - \eta \lambda U_t.$$

In the new coordinate, we have

$$\begin{aligned} \tilde{U}_{t+1} &= U_{t+1} P_Y \\ &= U_t P_Y - \eta V_t (V_t^\top U_t - Y^\top) P_Y - \eta \lambda U_t P_Y \\ &= \tilde{U}_t - \eta \tilde{V}_t Q_Y^\top (Q_Y \tilde{V}_t^\top \tilde{U}_t - Q_Y \Sigma_Y^T) - \eta \lambda \tilde{U}_t \\ &= \tilde{U}_t - \eta \tilde{V}_t (\tilde{V}_t^\top \tilde{U}_t - \Sigma_Y^T) - \eta \lambda \tilde{U}_t. \end{aligned} \tag{5}$$

On the other hand, since the Frobenius norm is invariant under left- or right-multiplication by orthogonal matrices, the loss function in the new coordinates is given by

$$\begin{aligned}\tilde{L}(\tilde{U},\tilde{V}) &= \frac{1}{2}\|P_Y\tilde{U}^\top\tilde{V}Q_Y^\top - Y\|_F^2 + \frac{\lambda}{2}(\|\tilde{U}P_Y^\top\|_F^2 + \|\tilde{V}Q_Y^\top\|_F^2)\\ &= \frac{1}{2}\|\tilde{U}^\top\tilde{V} - \Sigma_Y\|_F^2 + \frac{\lambda}{2}(\|\tilde{U}\|_F^2 + \|\tilde{V}\|_F^2).\end{aligned}$$

Note the update iteration (5) coincides with the $\tilde{U}$-update in minimizing $\tilde{L}(\tilde{U},\tilde{V})$ with gradient descent. An analogous calculation shows the same holds for the $\tilde{V}$-update. Therefore, one may directly study the gradient descent dynamics in minimizing $\tilde{L}(\tilde{U},\tilde{V})$.

D Quotient dynamics of gradient descent

We show that the gradient descent dynamics in the scalar factorization problem can be described by a quotient system, and we further establish key properties of this system.

Consider the map

$$T\colon \mathbb{R}^{2d} \to \mathbb{R}^2,\ T(u,v) = (u^\top v - y, \|u\|^2 + \|v\|^2).$$

Note that this definition differs from the one introduced in Section 3.2 by a constant shift of $-y$, where $y \in \mathbb{R}$ is target scalar of problem (2). This adjustment is made purely for convenience in presenting the proof. All results stated here extend trivially to the original formulation.

We will show that the gradient descent dynamics are fully captured by their evolution across the fibers of the map T. In other words, different initializations in the same fiber produce qualitatively identical trajectories. This reflects an inherent symmetry of the system. The quotient system factors out this symmetry and describes the fiber-wise dynamics. The term *quotient dynamical system* is borrowed from the theory of equivariant dynamical systems (see, e.g., Golubitsky and Stewart, 2003).

D.1 Quotient dynamical system

We first introduce two properties of the map T: (i) the preimage of any measure zero set has measure zero and (ii) the fiber of T is generically a smooth manifold.

Proposition 6. *The preimage of any measure-zero set under the map T is a measure-zero set.*

Proof. By Ponomarev (1987), it suffices to show the map T is a submersion almost everywhere, i.e., the Jacobian of T has rank two almost everywhere. Notice that

$$JT(u,v) = \begin{pmatrix} v & u \\ 2u & 2v \end{pmatrix}.$$

Hence, $\operatorname{rank}(JT) < 2$ if and only if there exists $c \neq 0$ such that $cv = 2u$ and $cu = 2v$. This gives $c^2v = 2cu = 4v$, and hence, $c = \pm 2$ or $v = 0$. The set $\{v = 0\}$ has zero measure. When $c = \pm 2$, we have $u = \pm v$ which also yields measure-zero set. This completes the proof. □

Proposition 7. *For almost all $(z,w) \in T(\mathbb{R}^{2d}) = \{(z,w) \in \mathbb{R}^2 \colon w \geq 2|z+\mu|\}$, $T^{-1}(z,w)$ is diffeomorphic to $\mathbb{S}^{d-1} \times \mathbb{S}^{d-1}$.*

Proof. Notice that

$$\|u+v\|_2^2 = w + 2(z+\mu), \quad \|u-v\|_2^2 = w - 2(z+\mu).$$

Consider the linear bijection $p = u + v$ and $q = u - v$. It follows that

$$T^{-1}(z,w) = \left\{(p,q)\colon \|p\|_2^2 = w + 2(z+\mu), \|q\|_2^2 = w - 2(z+\mu)\right\}.$$

Thus, the fiber is diffeomorphic to $\mathbb{S}^{d-1} \times \mathbb{S}^{d-1}$ whenever $w \pm 2(z+\mu) \neq 0$. Note this only fails at a measure-zero set, which completes the proof. □

Next, we prove Proposition 2. In the terminology of dynamical systems, this result shows that the gradient descent system GD_η is semi-conjugate to a planar system f under the map T.

Proposition 8 (Proposition 2). *Let $(u_t, v_t)_{t\geq 0}$ denote the gradient descent trajectory in problem* (4) *with $\lambda \geq 0$. Let $(z_t, w_t) = T(u_t, v_t)$. Consider the map $f\colon \mathbb{R}^2 \to \mathbb{R}^2$ defined by*

$$f\begin{pmatrix} z \\ w \end{pmatrix} = \begin{pmatrix} \eta^2 z^3 + \eta^2 y z^2 + ((1-\eta\lambda)^2 - \eta w + \eta^2\lambda w)z + y\eta^2\lambda^2 - 2y\eta\lambda \\ ((1-\eta\lambda)^2 + \eta^2 z^2)w - 4\eta z(1-\eta\lambda)(z+y) \end{pmatrix}. \tag{6}$$

We have that $(z_{t+1}, w_{t+1}) = f(z_t, w_t)$ holds for all $t \geq 0$. In particular, (u_t, v_t) converges to $\{u^\top v = y\}$ if and only if (z_t, w_t) converges to $\{z = 0\}$, and it converges to $(\mathbf{0}, \mathbf{0})$ if and only if (z_t, w_t) converges to $(-y, 0)$.

Proof. To ease the notation, let $(z, w) = (z_t, w_t)$ and $(z', w') = (z_{t+1}, w_{t+1})$ for arbitrary t. We have that

$$\begin{aligned} z' &= (u')^\top v' - y \\ &= (u - \eta z v - \eta\lambda u)^\top (v - \eta z u - \eta\lambda v) - y \\ &= z - \eta z w - 2\eta\lambda u^\top v + \eta^2 z^2 u^\top v + \eta^2\lambda z w + \eta^2\lambda^2 u^\top v \\ &= z - \eta z w - 2\eta\lambda(z+y) + \eta^2 z^2(z+y) + \eta^2\lambda z w + \eta^2\lambda^2(z+y) \\ &= \eta^2 z^3 + \eta^2 y z^2 + ((1-\eta\lambda)^2 - \eta w + \eta^2\lambda w)z + y\eta^2\lambda^2 - 2y\eta\lambda. \end{aligned}$$

Also, we have that

$$\begin{aligned} w' &= \|u'\|^2 + \|v'\|^2 \\ &= (u - \eta z v - \eta\lambda u)^\top (u - \eta z v - \eta\lambda u) + (v - \eta z u - \eta\lambda v)^\top (v - \eta z u - \eta\lambda v) \\ &= ((1-\eta\lambda)^2 + \eta^2 z^2)w - 4\eta z(1-\eta\lambda)(z+y). \end{aligned}$$

Note that, the loss function solely depends on $u^\top v - y$. Thus (u_t, v_t) converges to $\{u^\top v = y\}$ if and only if (z_t, w_t) converges to $\{z = 0\}$. Also, note that, $T(u, v) = (-y, 0)$ if and only if $u = v = \mathbf{0}$. Thus (u_t, v_t) converges to $(\mathbf{0}, \mathbf{0})$ if and only if (z_t, w_t) converges to $(-y, 0)$. This completes the proof. □

To further simplify the analysis, we consider the change of coordinates $\phi(z, w) = (\eta z, \eta w)$. Note that, under the map $\phi(z, w) = (\eta z, \eta w)$, the system f, as defined in (6), is topologically conjugate to

$$\begin{aligned} F\begin{pmatrix} z \\ w \end{pmatrix} = \phi \circ f \circ \phi^{-1}\begin{pmatrix} z \\ w \end{pmatrix} &= \begin{pmatrix} z^3 + \eta y z^2 + ((1-\eta\lambda)^2 - w + \eta\lambda w)z + y\eta^3\lambda^2 - 2y\eta^2\lambda \\ ((1-\eta\lambda)^2 + z^2)w - 4z(1-\eta\lambda)(z+\eta y) \end{pmatrix} \\ &= \begin{pmatrix} z^3 + \mu z^2 + ((1-\nu)^2 - w + \nu w)z + \nu^2\mu - 2\mu\nu \\ ((1-\nu)^2 + z^2)w - 4z(1-\nu)(z+\mu) \end{pmatrix}, \end{aligned} \tag{7}$$

where we let $\mu = \eta y$ and $\nu = \eta\lambda$. With Cauchy-Schwartz inequality, it is straightforward to verify that the state space of F is

$$\Omega = \left\{(z, w) \in \mathbb{R}^2 \colon w \geq 2|z + \mu|\right\}.$$

The system F has two parameters, μ and ν, whereas f has three, η, y, λ. Therefore, we instead study the system F. Note, trajectories of F and those of f only differ by a scale. Thus all results for F extend trivially to f.

D.2 Properties of the quotient dynamics

We show that the map F, as defined in (7), is a proper map, i.e., the preimage of any compact set is compact.

Proposition 9 (Properness). *When $0 \leq \nu < 1 - |\mu|$, the map F is proper on Ω.*

Proof. Consider $\|(z_k, w_k)\| \to \infty$ for a sequence of points (z_k, w_k). Let $(z'_k, w'_k) = F(z_k, w_k)$. Assume (z'_k, w'_k) stays bounded. Since (z_k, w_k) is unbounded and Ω is a cone, one must have $w_k \to \infty$. Notice that

$$w'_k = ((1-\nu)^2 + z_k^2)w_k - 4z_k(1-\nu)(z_k + \mu).$$

To make w_k' bounded, z_k has to be unbounded. However, as $w_k \geq 2|z_k + \mu|$,

$$\begin{aligned} w_k' &\geq ((1-\nu)^2 + z_k^2)w_k - 4|z_k| \cdot |z_k + \mu| \cdot |1-\nu| \\ &\geq ((1-\nu)^2 + z_k^2)w_k - 2|z_k| \cdot w_k \cdot |1-\nu| \\ &\geq w_k(|z_k| - (1-\nu))^2. \end{aligned}$$

Since $w_k, |z_k|$ are unbounded, w_k' has to be unbounded, which yields a contradiction. This completes the proof. □

Consider the function Q defined as follows

$$Q\colon \Omega \to \mathbb{R},\ Q(z,w) = w + \sqrt{w^2 - 16\mu z}.$$

We will frequently use Q as a Lyapunov-like function to study the dynamics of F.

In the following result, we describe the level set structure of the function Q.

Lemma 10 (Level-set structure)**.** *Consider $Q(z,w) = w + \sqrt{w^2 - 16\mu z}$. Then, $Q(z,w) \geq 4|\mu|$ for all $(z,w) \in \Omega$. Moreover, we have that*

- *If $r = 4|\mu|$, then for all $(z,w) \in \Omega$, $Q(z,w) = r$ if and only if $w = 2\mathrm{sgn}(\mu)(z+\mu)$ and $w \leq 4|\mu|$; $Q(z,w) > r$ holds for all other points.*
- *If $r > 4|\mu|$, then for all $(z,w) \in \Omega$, $Q(z,w)$ is less than, equal to, larger than r if and only if $-16\mu z - r^2 + 2rw$ is less than, equal to, larger than 0, respectively.*

Proof. When $w \geq 2|z+\mu|$,

$$w^2 - 16\mu z \geq 4(z+\mu)^2 - 16\mu z = 4(z-\mu)^2 \geq 0.$$

Therefore, Q is well-defined in Ω.

When $\mu = 0$, we have that $Q(z,w) = 2w$. The claimed results clearly hold. In the sequel, consider $\mu \neq 0$. Let $r = Q(z,w) = w + \sqrt{w^2 - 16\mu z}$ and $s = w - \sqrt{w^2 - 16\mu z}$. Then we have $z = (rs)/(16\mu)$ and $w = (r+s)/2$. Notice that

$$r^2 - s^2 = (r+s)(r-s) = 2w \cdot 2\sqrt{w^2 - 16\mu z} \geq 0.$$

Since $w \geq 2|z+\mu|$, we have $w^2 \geq 4(z+\mu)^2$ and hence

$$\begin{aligned} &(\frac{r+s}{2})^2 \geq 4(\frac{rs}{16\mu} + \mu)^2 \\ \Leftrightarrow\ &(r^2 - 16\mu^2)(s^2 - 16\mu^2) \leq 0 \\ \Leftrightarrow\ &r \geq 4|\mu|,\ |s| \leq 4|\mu|. \end{aligned} \tag{8}$$

We have that for $(z,w) \in \Omega$,

$$\begin{aligned} &w + \sqrt{w^2 - 16\mu z} = 4|\mu| \\ \Leftrightarrow\ &\sqrt{w^2 - 16\mu z} = 4|\mu| - w \\ \Leftrightarrow\ &w^2 - 16\mu z = (4|\mu| - w)^2,\ w \leq 4|\mu| \\ \Leftrightarrow\ &w = 2\mathrm{sgn}(\mu)(z+\mu),\ w \leq 4|\mu|. \end{aligned}$$

Therefore,

$$\{Q(z,w) = 4|\mu|\} = \{w = 2\mathrm{sgn}(\mu)(z+\mu),\ w \leq 4|\mu|\} \subset \partial\Omega,$$

and $\{Q(z,w) > r\} = \Omega \setminus \{Q(z,w) = r\}$.

Now we consider $r > 4|\mu|$. When $w = 2(z+\mu)$, we have

$$-16\mu z - r^2 + 2rw = 0 \Leftrightarrow w = \frac{r + 4\mu}{2}.$$

When $w = -2(z+\mu)$, we have

$$-16\mu z - r^2 + 2rw = 0 \Leftrightarrow w = \frac{r-4\mu}{2}.$$

Therefore, the line $-16\mu z - r^2 + 2rw = 0$ intersect with $\partial\Omega$ at two points, whose w coordinates are $\frac{r\pm 4\mu}{2}$. Since $r > 4|\mu|$, we have that $\frac{r\pm 4\mu}{2} < r$ always holds. This implies that, for all $(z,w) \in \Omega \cap \{-16\mu z - r^2 + 2rw < 0\}$, we have $r - w > 0$. Thus, we have that for $(z,w) \in \Omega$ and $r > 4|\mu|$,

$$\begin{aligned} & w + \sqrt{w^2 - 16\mu z} < r \\ \Leftrightarrow\ & \sqrt{w^2 - 16\mu z} < r - w \\ \Leftrightarrow\ & w^2 - 16\mu z < (r-w)^2 \\ \Leftrightarrow\ & -16\mu z - r^2 + 2rw < 0. \end{aligned}$$

The above clearly hold when $<$ is changed to $>$. This completes the proof. □

We identifies three invariant sets of the quotient system F. Recall that, a set $S \subset \Omega$ is said to be an invariant set under F if $F(S) \subset S$.

Lemma 11 (Invariant boundary)**.** *The boundary $\partial\Omega$ consists of two lines: $\{w = 2(z+\mu), w \geq 0\}$ and $\{w = -2(z+\mu), w \geq 0\}$. Each of the lines is an invariant set of F. Meanwhile, when $0 \leq \nu < 1 - |\mu|$, the set $\{Q = 4|\mu|\}$ is invariant under F.*

Proof. Let $(z', w') = F(z, w)$. By direct computation, we have that

$$\begin{aligned} w' - 2(z'+\mu) &= (w - 2(z+\mu))(1+z-\nu)^2, \\ w' + 2(z'+\mu) &= (w + 2(z+\mu))(-1+z+\nu)^2. \end{aligned} \tag{9}$$

It follows that if $(z,w) \in \partial\Omega = \{w = \pm 2(z+\mu)\}$, $F(z,w) \in \partial\Omega$.

According to Lemma 10, $\{Q = 4|\mu|\} = \{w = 2\mathrm{sgn}(\mu)(z+\mu), w \in [0, 4|\mu|]\}$. When $w = 2\mathrm{sgn}(\mu)(z+\mu)$, we have that the w-update is given by

$$\begin{aligned} w' &= w\left(\left(\mathrm{sgn}(\mu)\frac{w}{2} - \mu\right)^2 + (1-\nu)^2\right) - 2w\left(\mathrm{sgn}(\mu)\frac{w}{2} - \mu\right)(1-\nu) \\ &= w(\frac{w}{2} - 1 + \nu - |\mu|)^2 \\ &\triangleq \kappa(w). \end{aligned}$$

We will analyze the image set of $\kappa([0, 4|\mu|])$. Clearly, the minimum of $\kappa([0, 4|\mu|])$ is $\kappa(0) = 0$. Let $A = -1 + \nu - |\mu|$. We have that $\kappa'(w) = 0$ if $w = -2A$ or $w = -2A/3$. Notice that when $0 \leq \nu < 1 - |\mu|$, we have $4|\mu| \leq -2A$. Therefore, the maximum of $\kappa([0, 4|\mu|])$ is either $\kappa(4|\mu|)$ or $\kappa(-2A/3)$. When $4|\mu| > -2A/3$, we have $(1-\nu)/5 < |\mu| \leq 1 - \nu$. Notice that

$$\kappa(\frac{-2A}{3}) = \frac{8(1-\nu+|\mu|)^3}{27}.$$

Viewing $\kappa(\frac{-2A}{3})$ as a cubic function of $|\mu|$, we have that, as $1 - \nu > 0$, $\kappa(\frac{-2A}{3})$ is convex on $(1-\nu)/5 < |\mu| \leq 1-\nu$. Therefore, to show $\kappa(\frac{-2A}{3}) < 4|\mu|$ for $(1-\nu)/5 < |\mu| \leq 1-\nu$, it suffices to show this holds when $\mu = (1-\nu)/5$ and $\mu = 1 - \nu$. Notice that

$$\frac{8}{27}((1-\nu) + \frac{1-\nu}{5})^3 \leq 4 \cdot \frac{1-\nu}{5} \Leftrightarrow (1-\nu)^2 \leq \frac{25 \cdot 27}{2 \cdot 6^3} \approx 1.56,$$

and that

$$\frac{8}{27}(1 - \nu + 1 - \nu)^3 < 4(1-\nu) \Leftrightarrow (1-\nu)^2 \leq \frac{27}{16},$$

which are all satisfied. Therefore, $\kappa(-2A/3) \leq 4|\mu|$ when $4|\mu| > -2A/3$. Meanwhile, we have

$$\kappa(4|\mu|) = 4|\mu|(|\mu| - 1 + \nu)^2 = 4|\mu|(|\mu| - a)^2.$$

Since $0 < |\mu| \leq a$ and $0 \leq a < 1$, $\kappa(4|\mu|) \leq 4|\mu|$. Therefore, the image set of $\kappa([0, 4|\mu|])$ is contained $[0, 4|\mu|]$. This means that the set $\{Q = 4|\mu|\}$ is invariant under F, which completes the proof. □

In the sequel, we present two important properties of the map F, which will be used in the proof of our main results. In the following result, we identify the region on which a single update of F leads to a decrease, or an increase in the value of Q.

Lemma 12 (Monotonicity region)**.** *Assume $0 \le \nu < 1 - |\mu|$. When $\nu = 0$, we have that, for $(z, w) \in \Omega$: (i) $Q(F(z, w)) = Q(z, w)$ if and only if (z, w) lies in the set*

$$Z \triangleq \{w = \mu z + 4\} \cup \{z = 0\} \cup \{w = 2\mathrm{sgn}(\mu)(z + \mu), w \le 4|\mu|\};$$

and (ii) If $(z, w) \notin Z$, we have $\Big(Q(F(z, w)) - Q(z, w)\Big) \cdot (w - \mu z - 4) > 0$.

When $\nu > 0$, we have that, for $(z, w) \in \Omega$, $Q(F(z, w)) \le Q(z, w)$ if and only if (z, w) lies in the set

$$\{z^2 \le -\nu^2 + 2\nu\} \cup \left\{w < -\frac{\mu(z^2 - 2\nu + \nu^2)}{z(\nu - 1)} - \frac{4z^2(\nu - 1)}{\nu^2 - 2\nu + z^2}, z^2 > -\nu^2 + 2\nu\right\}.$$

In particular, $Q(z, w) \ge F(Q(z, w))$ if $Q(z, w) < 8 - 4\nu$.

Proof. Let $(z', w') = F(z, w)$. Assume that $\mu > 0$. The case of $\mu < 0$ can be proved via a analogous procedure. Let $r = Q(z, w)$ and let $s = w - \sqrt{w^2 - 16\mu z}$. When $r = 4|\mu|$, we have that $Q(F(z, w)) = Q(z, w)$ always holds, by Lemma 11. Consider $r > 4|\mu|$. Using Lemma 10, we have that the sign of $Q(z', w') - Q(z, w)$ is the same as that of the inner product between the vector pointing from (z, w) to (z', w') and the normal vector $(-8\mu, Q(z, w))$ of the line $-16\mu z - Q(z, w)^2 + 2Q(z, w)w = 0$, which is given by

$$\begin{aligned}
&(-8\mu)(z' - z) + Q(z, w)(w' - w) \\
=& -8\mu(z^3 + \mu z^2 + (\nu^2 - 2\nu - w + \nu w)z + \nu^2\mu - 2\mu\nu) + \\
&\quad Q(z, w)((\nu^2 - 2\nu + z^2)w - 4z(1 - \nu)(z + \mu)) \qquad (10) \\
\propto& \mu^2(r^2 - 16\mu^2)(r^2 s^2 + 8rs^2(-1 + \nu) + 256\mu^2(-2 + \nu)\nu) \\
\propto& r^2 s^2 + 8\nu r s^2 - 8rs^2 + 256\mu^2\nu^2 - 512\mu^2\nu.
\end{aligned}$$

When $\nu = 0$, the above is equal to $s^2 r(r - 8)$. By noticing that $r > 4|\mu| > 0$, that the sign of $r - 8$ is the same as that of $w - \mu z - 4$ by Lemma 10, and that $s = 0$ if and only if $z = 0$, we have all the results for $\nu = 0$.

When $\nu > 0$, (10) has the same sign as

$$2\mu(z^2 + \nu^2 - 2\nu) - (1 - \nu)z(w - \sqrt{w^2 - 16\mu z}).$$

We have that for $(z, w) \in \Omega$,

$$\begin{aligned}
&\{2\mu(z^2 + \nu^2 - 2\nu) - (1 - \nu)z(w - \sqrt{w^2 - 16\mu z}) <\leq 0\} \\
=&\{z^2 \le -\nu^2 + 2\nu\} \cup \left\{w < -\frac{\mu(z^2 - 2\nu + \nu^2)}{z(\nu - 1)} - \frac{4z^2(\nu - 1)}{\nu^2 - 2\nu + z^2}, z^2 > -\nu^2 + 2\nu\right\}.
\end{aligned}$$

Next, we show that $\{Q < 8 - 4\nu\}$ is contained in the above set. Notice that $8 > 4(|\mu| + \nu)$ always holds when $0 \le \nu < 1 - |\mu|$. So $8 - 4\nu > 4|\mu|$ and, by Lemma 10, the level set $\{Q = 8 - 4\nu\}$ is on the line

$$w = \frac{8\mu}{8 - 4\nu} z + \frac{8 - 4\nu}{2}.$$

Then it suffices to show that when $z^2 > -\nu^2 + 2\nu$, the following holds

$$-\frac{\mu(z^2 - 2\nu + \nu^2)}{z(\nu - 1)} - \frac{4z^2(\nu - 1)}{\nu^2 - 2\nu + z^2} - \left(\frac{8\mu}{8 - 4\nu} z + \frac{8 - 4\nu}{2}\right) \ge 0. \qquad (11)$$

By direct computation, we have that the level set $\{Q = 8 - 4\nu\}$ intersects $\partial\Omega$ at $z = \pm(2 - \nu)$. Hence, by the cone structure of Ω, we have $z^2 < (2 - \nu)^2$ if $Q < 8 - 4\nu$. Therefore, multiplying

$z(z^2+\nu^2-2\nu)$ to both sides of the above inequality and assuming $z>0$, we have that the inequality is equivalent to

$$\begin{aligned}&\frac{\nu}{(\nu-2)(\nu-1)}\cdot(-z^2+(2-\nu)^2)\cdot(-\mu z^2+(4-6\nu+2\nu^2)z-\mu(-2\nu+\nu^2))\geq 0\\ \Leftrightarrow\ &(-z^2+(2-\nu)^2)\cdot(-\mu z^2+(4-6\nu+2\nu^2)z-\mu(-2\nu+\nu^2))\geq 0\\ \Leftrightarrow\ &-\mu z^2+(4-6\nu+2\nu^2)z-\mu(-2\nu+\nu^2))\geq 0.\end{aligned}\tag{12}$$

The symmetry axis of the parabola is $(\nu-1)(\nu-2)/\mu>0$. Since $1-\nu>\mu$, the symmetry axis lies in $(2-\nu,+\infty)$. Notice that

$$\begin{aligned}&-\mu z^2+(4-6\nu+2\nu^2)z-\mu(-2\nu+\nu^2)|_{z=\sqrt{-\nu^2+2\nu}}\geq 0\\ \Leftrightarrow\ &2(1-\nu)\sqrt{-\nu^2+2\nu}\geq 0,\end{aligned}$$

which is satisfied. Therefore, (12) holds and (11) holds. The case of $z<0$ can be proved with a similar procedure. Thus, we have that $\{Q<8-4\nu\}$ is inside the set $\{Q(z,w)\geq Q(F(z,w))\}$.

When $\mu=0$, $Q(z,w)=2w$. We have that

$$\begin{aligned}Q(F(z,w))-Q(z,w)&=w(z^2+(1-\nu)^2)-4z^2(1-\nu)-w\\&=4z^2(-1+\nu)+w(z^2-2\nu+\nu^2).\end{aligned}$$

It is straightforward to verify that the claimed results hold for this case. This completes the proof. □

In the following result, we characterize the preimage map of F, which in general is a multi-valued map.

Proposition 13 (Preimage structure)**.** *Assume $0\leq\nu<1-|\mu|$. Consider the sets*

$$\begin{cases}B=\{(z,w)\in\Omega^o\colon Q(z,w)>6-4\nu\}\\ A_0=\{(z,w)\in\Omega^o\colon z<\nu-1\}\\ A_2=\{(z,w)\in\Omega^o\colon z>1-\nu\}.\end{cases}$$

The restrictions $F|_{\mathrm{cl}(A_0)}$, $F|_{\mathrm{cl}(A_2)}$ are homeomorphisms onto Ω. Moreover, there exists homeomorphisms $G_0\colon\Omega\to\mathrm{cl}(A_0)$, $G_1\colon\mathrm{cl}(B)\to G_1(\mathrm{cl}(B))\subset\{(z,w)\in\Omega\colon|z|\leq 1-\nu\}$, $G_2\colon\Omega\to cl(A_2)$ such that $F\circ G_i$ is an identity map on the domain of G_i for $i=0,1,2$.

Proof. Notice that the singular value of F lies in the set

$$\left\{\det JF(z,w)=-(1+z-\nu)(-1+z+\nu)(1-w-3z^2-2z\mu-2\nu+w\nu+\nu^2)=0\right\}.\tag{13}$$

Since $|\mu|<1-\nu$, the bottom tip of Ω, $(-\mu,0)$, lies in $(\nu-1,1-\nu)$. Therefore, A_0 is bounded by $w=-2(z+\mu)$ and $z=\nu-1$. Notice that the parabola $1-w-3z^2-2z\mu-2\nu+w\nu+\nu^2=0$ intersects $w=-2(z+\mu)$ at $z=(-2\mu-1+\nu)/3$ and we have

$$(-2\mu-1+\nu)/3>\nu-1\Leftrightarrow\mu+\nu<1,$$

which is satisfied by assumption. Therefore, $\det JF$ vanishes nowhere on A_0.

We next show that $F(A_0)=\Omega^o$. For an arbitrary $(z_0,w_0)\in\Omega^o$, $(z,w)\in F^{-1}(z_0,w_0)$ if (z,w) solves the following system

$$\begin{cases}z^3+\mu z^2+((1-\nu)^2-w+\nu w)z+\nu^2\mu-2\mu\nu=z_0\\((1-\nu)^2+z^2)w-4z(1-\nu)(z+\mu))=w_0.\end{cases}\tag{14}$$

For $z\neq 0$, solving (14) is equivalent to solving

$$w=\frac{z^3+\mu z^2+(1-\nu)^2z+\nu^2\mu-2\mu\nu-z_0}{(1-\nu)z}=\frac{4z(1-\nu)(z+\mu)+w_0}{z^2+(1-\nu)^2},$$

which is equivalent to solving the following quintic equation

$$\begin{aligned}p(z)=z^5+\mu z^4-2(\nu-1)^2z^3+((-2\nu^2+4\nu-3)\mu-z_0)z^2\\+(\nu-1)(\nu^3-3\nu^2+3\nu+w_0-1)z+(\nu-1)^2(\mu\nu(\nu-2)-z_0)=0.\end{aligned}\tag{15}$$

Notice that $p(-\infty) = -\infty$ and $p(-1) = (\nu - 1)^2(w_0 - 2(z_0 + \mu)) > 0$. Hence, p has at least one root in $(-\infty, -1)$. By Lemma 11, in particular, by (9), we have that, when viewing F as a map on $\mathbb{R}^2$:

$$F^{-1}(\partial\Omega) = \partial\Omega \cup \{z = \pm 1\}, \text{ and } F^{-1}(\Omega) \subset \Omega.$$

Therefore, the above root of p corresponds to one preimage in A_0. This means that $F(A_0) = \Omega^\circ$.

For any compact set $K \subset \Omega^o$. Note K is also compact in Ω. Since F is proper by Proposition 9, $F^{-1}(K)$ is compact. Since $K \cap \partial\Omega = \varnothing$ and $\partial(\Omega) \supset F(\partial A_0)$, we have $F^{-1}(K) \cap \partial A_0 = \varnothing$. Therefore, $(F|_{A_0})^{-1}(K) = F^{-1}(K) \cap A_0 = F^{-1}(K) \cap \mathrm{cl}(A_0)$, which is a closed in $F^{-1}(K)$. As a closed subset of a compact space is compact, we have $(F|_{A_0})^{-1}(K)$ is compact. Hence, $F|_{A_0}$ is a proper map. Since Ω^o is simply-connected, by Hadamard Inverse Function theorem, we have that $F|_{A_0}$ is a homeomorphism from A_0 to Ω^o.

We now show that F maps ∂A_0 bijectively to $\partial\Omega$. Since $A_0 \subset \mathrm{cl}(A_0)$, we have that $F(A_0) = \Omega^o \subset F(\mathrm{cl}(A_0))$. Since $\mathrm{cl}(A_0)$ is compact, therefore, $F|_{\mathrm{cl}(A_0)} \colon \mathrm{cl}(A_0) \to \Omega$ is proper, and hence is closed (see, e.g., Theorem 4.95. Lee, 2000). Therefore, $F(\mathrm{cl}(A_0))$ is a closed set that contains Ω^o. Hence, $\mathrm{cl}(\Omega^o) = \Omega \subset F(\mathrm{cl}(A_0))$. Since $F(A_0) = \Omega^o$, we have $\partial\Omega \subset F(\partial A_0)$, which means $F|_{\partial A_0}$ is onto $\partial\Omega$. By Lemma 11, we know F maps $\{z = \nu - 1\}$ to $\{w = 2(z + \mu)\}$ and maps $\{w = -2(z + \mu)\}$ to itself. When $z = \nu - 1$, the w-update is given by

$$w' = w((1 - \nu)^2 + (-1 + \nu)^2) - 4(1 - \nu)(-1 + \nu)(-1 + \mu + \nu),$$

which is linear in w. Therefore, $F|_{z=1-\nu}$ must be an injection. When $w = -2(z + \mu)$, the w-update is given by

$$w' = w(\frac{w}{2} - 1 + \mu + \nu)^2.$$

As a function w, w' have two critical points, $w = 2(1 - \mu - \nu)$ and $w = \frac{2}{3}(1 - \mu - \nu)$. Notice that $z = \nu - 1$ intersects $\partial\Omega$ at $(\nu - 1, 2(1 - \mu - \nu))$. Then when $(z, w) \in \mathrm{cl}(A_0)$, we have $w \geq 2(1 - \mu - \nu)$. Since $1 - \mu - \nu > 0$, we have that the above w' is monotonic with w. Therefore, $F|_{\mathrm{cl}(A_0)}$ is an injection. It follows that, $F|_{\partial A_0}$ is a bijection to $\partial\Omega$ and $F|_{\mathrm{cl}(A_0)}$ is a bijection to Ω. Note, $F|_{\mathrm{cl}(A_0)}$ is proper by Proposition 9 and by $\mathrm{cl}(A_0)$ is closed. Hence, $F|_{\mathrm{cl}(A_0)}$ is a closed map (see, e.g., Theorem 4.95. Lee, 2000), which means its inverse is continuous. Hence, $F|_{\mathrm{cl}(A_0)}$ is a homeomorphism. The proof for A_2 is similar and thus is omitted.

Finally, we analyze the behavior of F, as a map onto B. We show that every points in B are regular values. Note that,

$$\begin{aligned} & 6 - 4\nu - \frac{1 - 3z^2 - 2z\mu - 2\nu + \nu^2}{1 - \nu} > 0 \\ \Leftrightarrow\ & 3z^2 + 2\mu z + (3\nu^2 - 8\nu + 5) > 0. \end{aligned}$$

For this parabola, we have

$$\begin{aligned} & (2\mu)^2 - 4 \cdot 3(3\nu^2 - 8\nu + 5) < 0 \\ \Leftrightarrow\ & |\mu|^2 < 3(3\nu - 5)(\nu - 1) \\ \Leftarrow\ & (1 - \nu)^2 < -3(3\nu - 5)(1 - \nu) \\ \Leftarrow\ & \nu < \frac{7}{4}. \end{aligned}$$

So the parabola is always above $y = 0$. Therefore, we have that

$$\begin{aligned} & Q(z, \frac{1 - 3z^2 - 2z\mu - 2\nu + \nu^2}{1 - \nu}) < 6 - 4\nu \\ \Leftrightarrow\ & \sqrt{(\frac{1 - 3z^2 - 2z\mu - 2\nu + \nu^2}{1 - \nu})^2 - 16\mu z} < 6 - 4\nu - \frac{1 - 3z^2 - 2z\mu - 2\nu + \nu^2}{1 - \nu} \\ \Leftrightarrow\ & -16\mu z + 2(6 - 4\nu) \cdot \frac{1 - 3z^2 - 2z\mu - 2\nu + \nu^2}{1 - \nu} - (6 - 4\nu)^2 < 0 \\ \Leftrightarrow\ & (6\nu - 9)z^2 + 2\mu(4\nu - 5)z + (2\nu^3 - 9\nu^2 + 13\nu - 6) < 0. \end{aligned}$$

For this new parabola, we have its discriminant is negative if

$$\begin{aligned}&\mu^2(5-4\nu)^2-12(3-2\nu)^2(\nu^2-3\nu+2)<0\\ \Leftrightarrow\ &(1-\nu)^2(5-4\nu)^2-12(3-2\nu)^2(\nu-1)(\nu-2)<0\\ \Leftrightarrow\ &32\nu^3-182\nu^2+331\nu-191<0.\end{aligned}$$

By differentiation computation, we claim that the last equation holds when $\nu\in[0,1]$. Therefore, we prove that the maximum Q value on the parabola $\iota\colon 1-w-3z^2-2z\mu-2\nu+w\nu+\nu^2=0$ is at most $6-4\nu$. Notice that all the singular values of F is given by $\partial\Omega\cup F(\iota)$. But what we have shown and Lemma 12, we have

$$Q(z,w)\le 6-4\nu,\ \forall(z,w)\in F(\iota).$$

Therefore, we have that every points in B are regular values.

Now we show that $|F^{-1}(z,w)|=3$ for $(z,w)\in B$. To this end, we first consider a special point: $x^*=(-\mu+\mu(1-\nu)^2,w^*(1-\nu)^2)=F(0,w^*)$ for some w^* such that $x^*\in B$. Notice that the w-coordinate of x^* tends to infinity as w^* tends to infinity. Hence, w^* can be arbitrarily large while keeping $x^*\in B$, i.e., $Q(x^*)>6-4\nu$. We show that $|F^{-1}(x^*)|=3$. Plugging $z_0=-\mu+\mu(1-\nu)^2$ and $w_0=w^*(1-\nu)^2$ to (15) gives

$$\begin{aligned}&0=z^4+\mu z^3-2(\nu-1)^2z^2-3\mu(\nu-1)^2z+(\nu-1)^3(-1+\nu+w^*)\\ \Leftrightarrow\ &z^4+\mu z^3=(\nu-1)^2(2z^2+3\mu z-(\nu-1)(-1+\nu+w^*)).\end{aligned}\tag{16}$$

The left-hand side is a continuous function and thus has a finite upper bound when $z\in[-1+\nu,1-\nu]$. The right-hand side is a parabola, whose symmetry axis is at $-3\mu/4$. Hence, it's global minimum is

$$-\frac{9}{8}\mu^2(\nu-1)^2-(\nu-1)^3(-1+\nu+w^*).$$

Notice that this quantity tends to $+\infty$ as w^* tends to $+\infty$. Hence, for large enough w^*, equation (16) does not have a solution on $[-1+\nu,1-\nu]$. It follows that $F^{-1}(x^*)$ does not have any element in $\{z\in[-1+\nu,1-\nu]\}$ except $(0,w^*)$. By what we have shown, $F|_{\mathrm{cl}(A_0)}$ and $F|_{\mathrm{cl}(A_2)}$ are bijections onto Ω. Hence, $F^{-1}(x^*)$ have exactly one element in A_0 and exactly one in A_2. Therefore, $|F^{-1}(x^*)|=3$. Now consider any other point in B and a path connecting x^* and that point. Since every point in B is a regular value, by the stack of records theorem, the function $|F^{-1}(\cdot)|$ is locally constant. (Stack of records theorem requires the domain to be compact and this can be achieved by confining F on $w\le W$ for some large enough W so that the image contains the path. This is guaranteed by properness of F.) Note the path is compact and thus $|F^{-1}(z,w)|$ is a constant on the entire B and hence is 3.

Given $(z,w)\in B$, in $F^{-1}(z,w)$ we already know there are exactly one point in A_0 and exactly one point in A_2. Hence, the third point must lie in $\{(z,w)\in\Omega\colon|z|<1-\nu\}$. We define this map by $G_1\colon B\to\{(z,w)\in\Omega\colon|z|<1-\nu\}$ and let $A_1=G_1(B)$. By what we have shown, $\det JF$ vanishes nowhere on A_1. Note by construction of A_1, $F|_{A_1}(A_1)=B$. With a similar treatment as we used for A_0, we can show $F|_{A_1}$ is proper. As B is simply connected, we have that F, when restricted to A_1, is a homeomorphism to B. As we shown above, F is a bijection from $|z|=\pm(1-\nu)$ to $\partial\Omega$. Moreover, we claim that G_1 can be extended to $\{Q=6-4\nu\}$ in a bijective manner, as one can choose C slightly smaller than $6-4\nu$ and apply the same analysis for $\{(z,w)\in\Omega,|z|<1,Q>C\}$ as we did for B. Hence, F, when restricted to $\mathrm{cl}(A_1)$, is a bijection onto $\mathrm{cl}(B)$. Note, $F|_{\mathrm{cl}(A_1)}$ is proper and hence its inverse is continuous. Therefore, $F|_{\mathrm{cl}(A_1)}$ is a homeomorphism. This completes the proof. □

E Proofs for Section 3

In this section, we present the proofs of our main results. The key idea is to first analyze the quotient dynamical system introduced in Appendix D, and then translate the conclusions back to the original system.

E.1 Unregularized Problem

Preliminary results are first presented in Appendix E.1.1, and the proof of Theorem 1 is given in Appendix E.1.2.

E.1.1 PRELIMINARY RESULTS

As discussed in Appendix D, the gradient descent dynamics are captured by the following system F:

$$F\begin{pmatrix} z \\ w \end{pmatrix} = \begin{pmatrix} z^3 + \mu z^2 - zw + z \\ (z^2+1)w - 4z(z+\mu) \end{pmatrix},$$

where $\mu = y\eta$ denote the parameter of system F. Given $\eta > 0$, the state space of F is

$$\Omega = \{w \geq 2|z+\mu|\}.$$

In the following several results, we characterize the long term behavior of orbits of F. We will use the terms trajectory and orbit interchangeably. We say an orbit $\{x_k\}$ converges to a set S if $d(x_k, S) \to 0$, where $d(x, S) = \inf_{y\in S} d(x, y)$. Unless stated otherwise, we use (z', w') to denote $F(z, w)$.

Proposition 14 (Long-Term Dynamics)**.** *Assume $|\mu| \leq 1$. Given an initial condition $(z_0, w_0) \in \Omega$, we have that:*

- *If $w_0 < \mu z_0 + 4$, the orbit stays in $\{w < \mu z + 4\}$ and converges to*

$$\{w = 2\text{sgn}(\mu)(z+\mu), w \leq 4|\mu|\} \cup \{z = 0\}.$$

- *If $w_0 > \mu z_0 + 4$, the orbit either diverges, in the sense that $w_k \to \infty$ and $z_k \not\to 0$, or converges to $\{z = 0\}$ in finite steps.*
- *If $w_0 = \mu z_0 + 4$, the orbit stays in $\{w = \mu z + 4\}$.*

Proof. Consider function $\Delta Q(z, w) = Q(F(z, w)) - Q(z, w)$. When $w_0 < \mu z_0 + 4$, by Lemma 12, we have $Q(z_{k+1}, w_{k+1}) \leq Q(z_k, w_k)$ for all $k \geq 0$. Hence, the trajectory stays in the region $\{w < \mu z + 4\}$. Since $Q(z_k, w_k)$ is bounded from below, it converges to some finite value and $\Delta Q(z_k, w_k)$ converges to zero. Meanwhile, from Lemma 12,

$$\{\Delta Q = 0\} = Z = \{z = 0\} \cup \{w = \mu z + 4\} \cup \{w = 2\text{sgn}(\mu)(z+\mu), w \leq 4|\mu|\}.$$

If (z_k, w_k) does not converges to Z, there exists ε_0 such that for any K there exists $k > K$ such that $d((z_k, w_k), Z) \geq \varepsilon_0$. Note the function ΔQ is uniformly continuous on $\{w < \mu z + 4\} \subset \{w \leq \mu z + 4\}$ where the latter is compact. Hence, $d((z_k, w_k), Z) \geq \varepsilon_0$ implies that $\Delta Q(z_k, w_k) > \delta$ for some $\delta > 0$, which contradicts with the fact that $\Delta Q \to 0$. Therefore, (z_k, w_k) converges to

$$Z \cap \{w < \mu z + 4\} = \{z = 0\} \cup \{w = 2\text{sgn}(\mu)(z+\mu), w \leq 4|\mu|\}.$$

When $w_0 > \mu z_0 + 4$, similarly, we have that $Q(z_{k+1}, w_{k+1}) \geq Q(z_k, w_k)$. Hence, (z_k, w_k) stays in the region $\{w > \mu z + 4\}$ for all $k \geq 0$. Hence, $Q(z_k, w_k)$ either diverges to infinity or converges to a finite value. If it diverges, w_k must also diverge, since the function Q confined on $\{w \leq \bar{w}\}$ for any fixed $\bar{w}$, is continuous and hence upper bounded. Meanwhile, z_k can not converge to zero, since points on $\{z = 0\}$ are fixed points. If $Q(z_k, w_k)$ converges to some finite value C, then ΔQ converges to zero and the trajectory must remain within the region $\{w \leq C'\}$ for some $C' > 0$. Since ΔQ is uniformly continuous on $\{w \leq 2C'\}$, we have (z_k, w_k) converges to Z, using similar arguments as before. Hence, (z_k, w_k) can only converges to $Z \cap \{w > \mu z + 4\} = \{z = 0\}$. Now assume the convergence is in infinite steps, i.e., $|z_k| \neq 0$ for all $k \in \mathbb{N}$. Then the sequence $|z_{k+1}/z_k|$ is well defined and converges to one. Notice that we have

$$|\frac{z_{k+1}}{z_k}| = |z_k^2 + \mu z_k - w_k + 1| \geq |z_k^2 + \mu z_k| + |w_k - 1|.$$

Since $|z_k^2 + \mu z_k| \to 0$, the lower bound is dominated by $|w_k - 1|$ which is strictly greater than one since $\{w > \mu z + 4\} \cap \{z = 0\} = \{(0, w) \colon w \geq 4\}$. This contradicts with the fact that $|z_{k+1}/z_k|$ converges to one and hence the convergence must be in finite steps.

Finally, the result for the case $w_0 = \mu z_0 + 4$ directly comes from Lemma 12. With this, we conclude the proof. □

Proposition 15 (Convergence). *When $|\mu| > 1$, almost all initializations does not converge to $\{z = 0\}$. When $|\mu| < 1$, almost all initializations with $Q(z, w) < 8$ converges and almost all initializations with $Q(z, w) > 8$ diverges.*

Proof. First, consider $|\mu| < 1$. By Proposition 14, when $Q(z, w) > 8$, initializations either converge to $\{z = 0\}$ in finite steps or diverge. Notice that converging within finite steps means the initialization lies in the set

$$\cup_{N=0}^{\infty} F^{-N}(\{z = 0\}).$$

As the Jacobian of F has full rank almost everywhere, the above set is a null set. Hence, almost all initializations with $Q > 8$ diverge. When $Q < 8$, we have that the orbit converges to $\{z = 0\}$ or to $\{Q = 4|\mu|\} = \{w = 2\mathrm{sgn}(\mu)(z + \mu), w \le 4|\mu|\}$. Notice that, when $w = 2\mathrm{sgn}(\mu)(z + \mu)$, the w-update is given by

$$w' = \kappa(w) = \frac{1}{4} w \Big(w - 2 - 2|\mu| \Big)^2.$$

When confined on $w \in [0, 4|\mu|]$, the above map has two fixed point $w = 0, w = 2|\mu|$. It's easy to verify that, when $|\mu| < 1$, $w = 0$ is repelling, $w = 2|\mu|$ is attracting, and all orbits in this one-dimensional system converges to $w = 2|\mu|$ except that with initial value $w = 0$. Note $w = 0$ corresponds to the fixed point $(-\mu, 0)$ of F. The Jacobian of F at $(-\mu, 0)$ has eigenvalues $(1 + \mu)^2, (-1 + \mu)^2$. Therefore this point is a hyperbolic fixed point. By the local stable manifold theorem and the fact that $\{w = -\mathrm{sgn}(\mu)(z + \mu)\}$ is invariant under F, we have that the basin of attraction of $(-\mu, 0)$ can be given by

$$\cup_{N=0}^{\infty} F^{-N}(O \cap \{w = -\mathrm{sgn}(\mu)(z + \mu)\}),$$

for some small neighborhood O of $(-\mu, 0)$. Notice that this set is a null set, since the Jacobian of F has full rank almost everywhere. Therefore, for almost all initializations with $Q < 8$, we have that they converge to $\{z = 0\}$ or to $\{Q = 4|\mu|\}$, but not to $(-\mu, 0)$. Since $w = 2|\mu|$ attracts all orbits except $(-\mu, 0)$ on the invariant set $\{Q = 4|\mu|\}$, we have that all these orbits that converge to $\{Q = 4|\mu|\}$ but not to $(-\mu, 0)$ must converge to $(0, 2|\mu|) \in \{z = 0\}$. Hence, almost all initializations with $Q < 8$ converge to $\{z = 0\}$.

Now consider $|\mu| > 1$. We have that $\inf\{w \colon (0, w) \in \Omega\} = 2|\mu|$. Therefore, if $z \neq 0$,

$$|z'/z| = |z^2 + \mu z - w + 1| \ge |w - 1| > 1.$$

This implies that converging to any global minimizer can only occurs within finite steps, which is a measure-zero event as shown above. This completes the proof. □

Note, the above proof implies the following corollary.

Corollary 16. *Consider gradient descent with step η in problem* (2)*. Any global minimizer with $\|u\|^2 + \|v\|^2 \ge 2/\eta$ is an unstable minimizer, i.e., it repels orbits in its neighborhood. Consequently, initializations that converge to such as minimizer form a measure-zero set. Moreover, when $|\mu| > 1$, i.e., $\eta|y| > 1$, all global minimizers are unstable.*

Next, we analyze dynamics on the boundary $\{w = \mu z + 4\}$. By Proposition 14, the boundary is forward-invariant. Moreover, the system reduces to a one dimensional system

$$\tilde{F}(z) = z^3 + \mu z^2 - z(\mu z + 4) + z = z^3 - 3z, \quad z \in [-2, 2].$$

Proposition 17 (Chaotic Boundary Dynamics). *The system $\tilde{F}$ on $I = [-2, 2]$ is Devaney-chaotic and has topological entropy* $\log 3$*. Moreover, there exists periodic orbits with any period and thus $\tilde{F}$ is also Li-Yorke chaotic.*

Proof. We first seek a simpler system which is topologically conjugate to $\tilde{F}$. Notice that $\tilde{F}$ is a continuous map from $[-2, 2]$ to itself. Consider $\psi_0(z) = z/2$, which is a homeomorphism from $[-2, 2]$ to $[-1, 1]$, and $\tilde{F}_1(z) = 4z^3 - 3z$, which is a continuous map from $[-1, 1]$ to itself. We have that

$$\tilde{F}_1 \circ \psi_0(z) = 4(\frac{z}{2})^3 - \frac{3z}{2} = \frac{z^3}{2} - \frac{3z}{2} = \psi_0 \circ \tilde{F}(z).$$

Hence, $\tilde{F}$ is conjugate to $\tilde{F}_1$. Now consider $\psi(z) = \sin(\frac{\pi}{2} \cdot z)$, which is a homeomorphism from $[-1, 1]$ to $[-1, 1]$, and

$$\tilde{F}_2(z) = \begin{cases} 3z + 2, & x \in [-1, -1/3]; \\ -3z, & x \in (-1/3, 1/3); \\ 3z - 2, & x \in [1/3, 1], \end{cases}$$

which is a continuous map from $[-1, 1]$ to $[-1, 1]$. We have that for $z \in [-1, -1/3]$,

$$\tilde{F}_1 \circ \psi(z) = 4\sin^3(\frac{\pi}{2} \cdot z) - 3\sin(\frac{\pi}{2} \cdot z) = -\sin(\frac{3\pi}{2}z) = \sin(\frac{\pi}{2}(3z + 2)) = \psi \circ \tilde{F}_2(z).$$

Similarly, one can verify that $\tilde{F}_1 \circ \psi = \psi \circ \tilde{F}_2$ also holds on $(-1/3, 1/3)$ and $[1/3, 1]$. Hence, $\tilde{F}_2$ is topologically conjugate to $\tilde{F}$, and $\tilde{F}$ is chaotic if and only if $\tilde{F}_2$ is (Elaydi, 2007, Theorem 3.9,).

Note $\tilde{F}_2$ is a piecewise linear continuous map with slope equal to ± 3. Hence, the topological entropy of $\tilde{F}_2$ is equal to $\log 3$ (De Melo and Van Strien, 2012, Corollary of Theorem 7.2,). For univariate map on a compact interval, positive topological entropy implies Devaney-chaotic (Theorem 3.13, Elaydi, 2007). Also, topological conjugacy preserves topological entropy (Theorem 1.7, Ch.8, Robinson, 1998). Therefore, we have $\tilde{F}$ is Devaney chaotic and has topological entropy $\log 3$.

We now show the existence of periodic orbit with any period. According to the Li-Yorke Theorem (Li and Yorke, 1975), a sufficient condition is that there exists a point x such that $\tilde{F}_2^3(x) \leq x < \tilde{F}_2(x) < \tilde{F}_2^2(x)$. Such point can be found explicitly. Consider $x = -5/7$. We have that $f(x) = -1/7$, $f^2(x) = 3/7$, and $f^3(x) = -5/7$. This completes the proof. □

The topological entropy of the boundary dynamics provide a lower bound of the original gradient descent dynamics.

Proposition 18. *The set $\partial\mathcal{D}'_\eta$ is invariant under GD_η. We have that*

$$h(\mathrm{GD}_\eta) \geq h(\mathrm{GD}_\eta|_{\partial\mathcal{D}_\eta}) \geq \log 3.$$

Proof. By Lemma 12, $\partial\mathcal{D}'_\eta$ is invariant under GD_η. Notice that the map $(u, v) \mapsto (z, w)$ is a semi-conjugacy between $\mathrm{GD}_\eta|_{\partial\mathcal{D}_\eta}$ and $\tilde{F}$. Therefore, with Theorem 1.7, Chapter 8 in Robinson (1998) we have $h(\mathrm{GD}_\eta|_{\partial\mathcal{D}_\eta}) \geq h(\tilde{F}) = \log 3$. Since $\partial\mathcal{D}'_\eta$ is an invariant subset, with Proposition 8.1.7 in Vries (2014), we have that $h(\mathrm{GD}_\eta) \geq h(\mathrm{GD}_\eta|_{\partial\mathcal{D}_\eta})$, which completes the proof. □

In the following, we show that, the original gradient descent system is not chaotic in the sense of Devaney when $d \geq 2$.

Proposition 19. *When $d \geq 2$, the system $\mathrm{GD}_\eta|_{\partial\mathcal{D}_\eta}$ is not topological transitive.*

Proof. Notice that

$$u' + v' = u - \eta z v - \eta\lambda u + v - \eta z u - \eta\lambda v = (1 - \eta z - \eta\lambda)(u + v).$$

Therefore, $u_k + v_k$ is always parallel to $u_0 + v_0$. Consider the map $\tau \colon \mathbb{R}^{2d} \to \mathbb{S}^{d-1} \times \mathbb{S}^{d-1}$:

$$\tau(u, v) = \left(\frac{u + v}{\|u + v\|}, -\frac{u + v}{\|u + v\|} \right).$$

For any open set $A \subset \mathbb{R}^{2d}$, we have $\tau(A) = \tau(\mathrm{GD}_\eta^N(A))$ for all $N \geq 0$. Since $d \geq 2$, we can always choose two open sets $A, B \subset \mathbb{R}^{2d}$ small enough such that $\tau(A) \cap \tau(B) = \varnothing$. This means that $\tau(\mathrm{GD}_\eta^N(A)) \cap \tau(\mathrm{GD}_\eta^N(B)) = \varnothing$ for all $N \geq 0$. Since $\tau(\mathrm{GD}_\eta^N(A) \cap \mathrm{GD}_\eta^N(B)) \subset \tau(\mathrm{GD}_\eta^N(A)) \cap \tau(\mathrm{GD}_\eta^N(B))$, we have the former set is also empty. Hence, $\mathrm{GD}_\eta^N(A) \cap \mathrm{GD}_\eta^N(B)$ is empty. Therefore, GD^N is not topological transitive. This gives the claimed result. □

We proceed to show that when the initialization is near the boundary, the orbit can visit any point in the state space.

Proposition 20. *Assume $|\mu| < 1$. Given any $(z^*, w^*) \in \Omega$ and any open set $O \subset \Omega$ such that $O \cap \{Q(z,w) = 8\} \neq \varnothing$, there exists $N \geq 0$ and $(z,w) \in O$ such that $F^N(z,w) = (z^*, w^*)$.*

Proof. As in Proposition 13, let $G_0 \colon \Omega \to \mathrm{cl}(A_0)$ denote the inverse of $F|_{\mathrm{cl}(A_0)}$. Let $m_0 = (z^*, w^*)$ and $m_k = G_0^k(m_0)$ for $k \geq 1$. We show that $\lim_{k\to\infty} m_k = m^* = (-2, 4-2\mu)$. Note for all $k \geq 1$, $m_k \notin \{Q = 4|\mu|\}$. Therefore, by Lemma 12, we know that $Q(m_k)$ either stays at 8 or is monotonic. Hence, as we shown in the proof of Proposition 14, m_k must converge to

$$Z = \{\Delta Q = 0\} = \{z = 0\} \cup \{w = \mu z + 4\} \cup \{w = 2\mathrm{sgn}(\mu)(z+\mu), w \leq 4|\mu|\}\,.$$

Therefore, m_k must converge to the set $Z \cap A_0$. Intersecting Z with $\mathrm{cl}(A_0)$, we get

$$Z \cap A_0 = \{z \leq -1, w = \mu z + 4\}\,.$$

Notice that, when restricted to $\{w = \mu z + 4\}$, the system F reduces to $\tilde{F}(z) = z^3 - 3z, \quad z \in [-2, 2]$. Then $G_0|_{Z\cap A_0}$ corresponds to the branch of $\tilde{F}^{-1}$ whose image is $[-2, -1]$. Using the conjugacy we provided in Proposition 17, it's easy to obtain that $z = -2$ is the unique, globally attracting fixed point for the map $G_0|_{Z\cap A_0}$. Since m_k converges to $Z \cap A_0$ and $z = -2$ is globally attracting, we have that $m_k \to m^*$ as $k \to \infty$.

Now consider the given open set O which satisfies $O \cap \{Q = 8\}$ is not empty. We prove that there exists $x \in O$ and n such that $F^n(x) = m^*$. Notice that $F|_{\{Q=8\}}$ is topologically conjugate to the piece-wise linear map $\tilde{F}_2$ as we shown in the proof of Proposition 17. For $\tilde{F}_2$, the full preimage of the two endpoint of the interval $[-1, 1]$ is given by

$$\cup_{k\geq 0}\{-1 + \frac{2j}{3^k} \colon j = 0, 1, \cdots, 3^k\},$$

which is dense in $[-1, 1]$. Particularly, it is clear that the preimage of -1 is dense. Therefore, there exists $x \in O$ and n such that $F^n(x) = m^*$, i.e., $x \in F^{-n}(m^*)$. Notice $\{Q = 8\} \subset \mathrm{cl}(B)$, by Proposition 13, we have that there exists $i_1, \cdots, i_{n_1} \in \{0, 1, 2\}$ such that $G_{i_{n_1}} \circ \cdots \circ G_{i_1}(m^*) = x$. Since the composition of G_i's is continuous, there exists a neighborhood $\tilde{O}$ of m^* such that $G_{i_{n_1}} \circ \cdots \circ G_{i_1}(\tilde{O}) \subset O$. Since $m_k \to m^*$, there exists n_2 such that $m_{n_2} = G_0^{n_2}(0, w^*) \in \tilde{O}$. Taken together, we have that

$$G_{i_{n_1}} \circ \cdots \circ G_{i_1} \circ G_0^{n_2}(0, w^*) \triangleq \hat{m} \in O.$$

This implies that

$$F^{n_1+n_2}(\hat{m}) = (0, m^*),$$

which completes the proof. □

E.1.2 Proof of Theorem 1

Proof of Theorem 1. According to Proposition 6, any measure-zero event in system F corresponds to a measure-zero even in system GD_η. According to Proposition 8, the orbit of GD_η converges to $\{u^\top v = y\}$ if and only if the orbit of F converges to $\{z = 0\}$, and the former converges to $(\mathbf{0}, \mathbf{0})$ if and only the latter converges to $(-y, 0)$. According to Proposition 15, when $|\mu| < 1$ and for almost all initializations (z, w), the orbit converges to $\{z = 0\}$ if $Q(z, w) < 8$. Notice that $\mu = \eta y$ and due to the conjugacy (7),

$$\begin{aligned} Q(z,w) < 8 &\Leftrightarrow \eta(\|u\|_2^2 + \|v\|_2^2) + \sqrt{\eta^2(\|u\|_2^2 + \|v\|_2^2)^2 + 16\eta y \cdot \eta(u^\top v - y)} < 8 \\ &\Leftrightarrow (\|u\|_2^2 + \|v\|_2^2) + \sqrt{(\|u\|_2^2 + \|v\|_2^2)^2 + 16y \cdot (u^\top v - y)} < \frac{8}{\eta}. \end{aligned}$$

Also, when $Q(z, w) > 8$ or $|\mu| > 1$, almost all initializations do not converge. This gives the critical step size (3).

We now show the sensitivity to initialization. Consider any open neighborhood $W \subset \mathbb{R}^{2d}$ such that $W \cap \partial\mathcal{D}'_\eta \neq \varnothing$. Notice that the Jacobian of the map T drops rank if and only if $\{u = \pm v\}$. Also, we

have that

$$\begin{aligned}(u,v)\in\partial\mathcal{D}'_\eta &\Leftrightarrow \|u\|_2^2+\|v\|_2^2+\sqrt{(\|u\|_2^2+\|v\|_2^2)^2-16y(u^\top v-y)}=\frac{8}{h}\\ &\Rightarrow 4=\eta(\|u\|_2^2+\|v\|_2^2)+\eta^2y(u^\top v-y)\\ &\Rightarrow (u^\top\ v^\top)\begin{pmatrix}\eta I & \eta^2y/2\\ \eta^2y/2 & \eta I\end{pmatrix}\begin{pmatrix}u\\ v\end{pmatrix}=4+\eta^2y^2.\end{aligned}$$

The last equation is a quadratic form, and the eigenvalues of the coefficient matrix are $\eta\pm\frac{1}{2}\eta^2|y|$, each with multiplicity d. Therefore, when $\eta|y|<1$, the quadratic form is positive definite and defines a smooth ellipsoid of dimension $2d-1$. Notice that, $\{u=\pm v\}$ is the union of two linear subspace with dimension d. Therefore, since $2d-1\geq 1$ and an ellipsoid is curved everywhere, there always exits a point $\bar\theta\in W\cap\partial\mathcal{D}'_\eta\setminus\{u=\pm v\}$ and a neighborhood $\bar W$ of $\bar\theta$ such that $\bar W\subset W$ and $\bar W\cap\{u=\pm v\}=\varnothing$. The Jacobian of T is full rank at all points in $\bar W$, so by constant rank theorem, $T(\bar W)$ is an open set. Meanwhile, $T(\bar\theta)\in T(\partial\mathcal{D}'_\eta)$. Hence, under the conjugacy (7), we have $T(\bar W)\cap\{w=\mu z+4\}\neq\varnothing$. According to Proposition 20, there exists $(z',w'),(z'',w'')\in T(\bar W)$ such that $F^N(z',w')$ converges to $(0,w^*)$ with any $w^*\in[2|\mu|,\infty)$ and $F^N(z'',w'')$ converges to $(-\mu,0)$, as N tends to infinity. Therefore, there exists $\theta',\theta''\in W$ such that $\mathrm{GD}_\eta^N(\theta')$ converges to a global minimizer with squared norm in $[2|y|,\infty)$ and $\mathrm{GD}_\eta^N(\theta'')$ converges to $(\mathbf{0},\mathbf{0})$. Notice that

$$\|u\|^2+\|v\|^2\geq 2\|u\|\cdot\|v\|\geq 2|u^\top v|.$$

Therefore, the minimal squared norm at $\{u^\top v=y\}$ is $2|y|$. Also, notice that

$$\begin{aligned}\|uu^\top-vv^\top\|_F^2&=\mathrm{Tr}((uu^\top-vv^\top)(uu^\top-vv^\top))\\ &=\|u\|^4+\|v\|^4-2(u^\top v)^2\\ &=(\|u\|^2+\|v\|^2)^2-2\|u\|^2\|v\|^2-2(u^\top v)^2\\ &\geq\frac{(\|u\|^2+\|v\|^2)^2}{2}-2(u^\top v)^2.\end{aligned}$$

Hence, at any global minimizer, the imbalance is lower bounded by the squared norm. Hence, by what we have shown, arbitrarily large imbalance can be also attained by initialization in $\bar W$.

Finally, the result of topological entropy and the existence of periodic orbit of any period directly come from Proposition 18. This completes the proof. □

Lastly, we present a basic property for the unregularized scalar factorization problem: the sharpness coincides with the squared norm at the set of global minimizers. This property has been proved by Wang et al. (2022).

Proposition 21 (Wang et al., 2022, Theorem F.2)**.** *For the unregularized scalar factorization problem* (2)*, the eigenvalues of the Hessian ∇^2L are $\pm(u^\top v-y)$, each with multiplicity $d-1$, and $\frac{1}{2}(\|u\|^2+\|v\|^2\pm\sqrt{(\|u\|^2+\|v\|^2)^2+4(u^\top v-y)^2+8(u^\top v-y)u^\top v})$. Consequently, when $u^\top v=y$, we have that*

$$\lambda_{\max}(\nabla^2L(u,v))=\mathrm{Tr}(\nabla^2L(u,v))=\|u\|^2+\|v\|^2.$$

E.2 Regularized Problem

Similar to the previous section, preliminary results are first presented in Appendix E.2.1, and the proofs of Theorem 3 and Theorem 4 is given in Appendix E.2.2.

E.2.1 Preliminary results

Unless stated otherwise, we use (z',w') to denote $F(z,w)$. We first show that when the step size is small enough, the quotient dynamics F is predictable.

Proposition 22 (Small step size)**.** *Assume $0<\nu<1-|\mu|$. For almost all $(z,w)\in\Omega$, if $Q(z,w)<8-4\nu$, we have that $F^N(z,w)$ converges to the global minimizer. If $Q(z,w)<4-4\nu$, we have that, for any (u,v) that satisfies $T(u,v)=(z,w)$, $\mathrm{GD}_\eta^N(u,v)$ converges to $p^-(u,v)$, as defined in Theorem 3.*

Proof. By Lemma 12, we have that $Q(F^N(z,w))$ monotonically decreases and converges to $\{\Delta Q = 0\} = \{Q = 4|\mu|\}$. As shown in proving Lemma 11, the w-update on $\{Q = 4|\mu|\}$ is given by

$$w' = \kappa(w) = w(\frac{w}{2} - 1 + v - |\mu|)^2.$$

By differentiation, when $|\mu| > \nu$, $\kappa(w)$ has two fixed points $w = 0$ and $w = 2(|\mu| - \nu)$ on $[0, 4|\mu|]$. In particular, $w = 0$ is repelling and $w = 2(|\mu| - \nu)$ is globally attracting, i.e., attracting all orbits on $[0, 4|\mu|]$ except $w = 0$. When $|\mu| \le \nu$, $\kappa(w)$ has only one fixed point $w = 0$ which is globally attracting. In either case, the attracting fixed points is the global minimizer and hence for almost all initializations, the orbit converges to the minimizer. The measure-zero event occurs if $|\mu| > \nu \ge 0$ and the initializations lies on the measure-zero set (it has measure zero since the Jacobian of F has full rank almost everywhere):

$$\cup_{N=0}^{\infty} F^{-N}(O \cap \{w = -2\mathrm{sgn}(\mu)(z + \mu)\}),$$

for some neighborhood O of $(-\mu, 0)$. Note, this set is the basin of attraction of the saddle $(-\mu, 0)$

Without loss of generality, assume $y \ge 0$. Consider $p = (u + v)/\sqrt{2}$ and $q = (u - v)/\sqrt{2}$. Note that when $y > \lambda$, the set of global minimizers is given by

$$\left\{u = v, \|u\|_2^2 = y - \lambda\right\} = \left\{q = 0, \|p\|^2 = 2(y - \lambda)\right\}.$$

Also, notice that

$$\sqrt{2}\cdot p' = u' + v' = u - \eta z v - \eta\lambda u + v - \eta z u - \eta\lambda v = (1 - \eta z - \eta\lambda)(u + v) = (1 - \eta z - \eta\lambda)\sqrt{2}\cdot p.$$

Under the conjugacy (7), we have

$$p_k = p_0 \Pi_{j=0}^{k-1}(1 - z_j - \nu). \tag{17}$$

Similarly,

$$q_k = q_0 \Pi_{j=0}^{k-1}(1 + z_j - \nu).$$

Therefore, the converged point is either $(\sqrt{2(y - \lambda)}\frac{p_0}{\|p_0\|}, 0)$ or $(-\sqrt{2(y - \lambda)}\frac{p_0}{\|p_0\|}, 0)$. Since the global minimizer is given by $\left\{q = 0, \|p\|^2 = 2(y - \lambda)\right\}$, the former is the minimal distance solution and the latter is the maximal distance solution. Note the change of coordinates $p = (u + v)/\sqrt{2}$ and $q = (u - v)/\sqrt{2}$ is given by an orthogonal transformation which preserves distance. Therefore the same statement holds in the uv-coordinate.

Note that,

$$Q(z, w) = 4 - 4\nu \Leftrightarrow -2\mu z - 2(1 - \nu)^2 + (1 - \nu)w = 0.$$

Note the line intersects with $\partial\Omega$ at $(1 - \nu, 2(1 - \nu + \mu))$ and $(\nu - 1, -2(\nu - 1 + \mu))$. Therefore we have that for all initializations that satisfy $Q(z, w) < 4 - 4\nu$, we have $|z| < 1 - \nu$. Meanwhile, since $4 - 4\nu < 8 - 4\nu$, we have that the $\{Q < 4 - 4\nu\}$ is forward invariant by Lemma 12, i.e., $|z| < 1 - \nu$ holds on the entire orbit. Therefore, when $Q(z, w) < 4 - 4\nu$, we have that $1 \pm z_j - \nu > 0$ for all $j \ge 0$. It follows that, by (17), the converged minimizer in pq-coordinate has to be $(\sqrt{2(y - \lambda)}\frac{p_0}{\|p_0\|}$, which is the minimal distance solution. This completes the proof. □

We now proceed to show the projected boundary $T(\partial\mathcal{D}_\eta'')$ is self-similar.

Proposition 23 (Self-similarity)**.** *Assume $0 < \nu < 1 - |\mu|$. The boundary $T(\partial\mathcal{D}_\eta'')$ is self-similar with degree three.*

Proof. We use $\mathcal{D}$ for $\mathcal{D}_\eta''$ for notation simplicity. First, we prove that $T(\partial\mathcal{D}_\eta'') = \partial T(\mathcal{D}_\eta'')$. Notice that, by Proposition 8, $T^{-1}(T(\mathcal{D})) = \mathcal{D}$, i.e., $\mathcal{D}$ is saturated with respect to T. Since T is continuous, we have that $\partial T^{-1}(A) \subset T^{-1}(\partial A)$ for any set A. Hence, $\partial T^{-1}(T(\mathcal{D})) = \partial\mathcal{D} \subset T^{-1}(\partial T(\mathcal{D}))$. It follows that, $T(\partial\mathcal{D}) \subset \partial T(\mathcal{D})$. By Proposition 22,

$$\Gamma = \left\{(u, v) \colon Q(T(u, v)) = \|u\|^2 + \|v\|^2 + \sqrt{(\|u\|^2 + \|v\|^2)^2 - 16y(u^\top v - y)} < 8 - 4\lambda\right\}$$

is an open set and all points in this set converge to the global minimizer or the saddle. Hence, $\mathcal{D}$ is an open set. To see this, if $x \in \mathcal{D}$ then we have for sufficiently large N, $\mathrm{GD}_\eta^N(x) \in \Gamma$. By the continuity of GD_η^N, we have x is in an interior point of $\mathcal{D}$. Now consider any point $y \in \partial T(\mathcal{D})$. For the sake of contradiction, assume $y \notin T(\partial\mathcal{D})$. Then we have $T^{-1}(y) \cap \partial\mathcal{D} = \varnothing$. Note $T^{-1}(y)$ is a compact set by the properness of T. Since $\mathcal{D}$ is open, there exists an open neighborhood O of $T^{-1}(y)$ such that $O \subset \mathcal{D}$ or $O \subset (\mathcal{D}^c)^o$. In either case, we have $y \in T(O)$ and $T(O) \cap T(\partial\mathcal{D}) = \varnothing$, which yields a contradiction. Hence $y \in T(\partial\mathcal{D})$ and $\partial T(\mathcal{D}) \subset T(\partial\mathcal{D})$. It follows that $\partial T(\mathcal{D}) = T(\partial\mathcal{D})$.

Next, we prove that, $F(\partial T(\mathcal{D})) = \partial T(\mathcal{D})$. Now let $A = T(\mathcal{D})$ for simplicity. First, note that A satisfies $F(A) \subset A$, $F^{-1}(A) \subset A$ by the definition of A. Consider any point x such that $T(x) \in \partial A$. Then any small enough neighborhood O of x is mapped a neighborhood of $T(x)$, which contains a point $y \in A$ and a point $z \in A^c$. Since $F^{-1}(A) \subset A$, $F^{-1}(y) \in O \cap A$. Since $F(A) \subset A$, $F^{-1}(z) \in A^c$. Therefore, we have that $F^{-1}(\partial A) \subset \partial A$. Meanwhile, since F is surjective by Proposition 13, we have $F \circ F^{-1}(\partial A) = \partial A$. It follows that

$$\partial A = F \circ F^{-1}(\partial A) \subset F(\partial A).$$

On the other side, for any $y \in \partial A$, since $y \in \mathrm{cl}(A)$ and F is continuous, we have that $T(y) \in \mathrm{cl}(F(A)) = \mathrm{cl}(A)$. Since $F^{-1}(A) \subset A$, $T(y) \notin A$. Hence, $T(y) \in \partial A$. This means that $F(\partial A) \subset \partial A$. Therefore, $F(\partial A) = \partial A$.

By proposition 22, we have that A contains $\{Q(z,w) < 8 - 4\nu\}$. Therefore, its boundary, ∂A, must lie in $\{Q \geq 6 - 4\nu\}$. Since $F(\partial A) = \partial A$, by Proposition 13, we have that

$$\partial T(\mathcal{D}_\eta'') = \cup_{k=0,1,2} G_i(\partial T(\mathcal{D}_\eta'')),$$

where G_i's are homeomorphisms. As shown in Proposition 13, $G_i(\Omega^o) \cap G_j(\Omega^o)$ is empty whenever $i \neq j$. Therefore, $\partial T(\mathcal{D}_\eta'')$ is self-similar with degree three. This completes the proof. □

In the following, we show that $\mathcal{D}_\eta$ is equal almost everywhere to a set with unbounded interior.

Proposition 24 (Unboundedness)**.** *When $\mu = 0, 0 \leq \nu < 1$, there exists $a, b > 0$ such that, for almost all initializations that lie in $\{(z,w) \in \Omega \colon |z| < a\exp(-bw)\}$, the orbit converges to the minimizer.*

Proof. Let $(z', w') = F(z, w)$. Note, when $\mu = 0$, the unique global minimizer of L corresponds to $(0, 0)$. Let $\alpha = 1 - \nu$. Then $0 < \alpha < 1$. Assume that $|z| < a\exp(-bw)$ for some $a, b > 0$. We aim to show that $|z'| < a\exp(-bw')$. Notice that

$$\begin{aligned} |z'| &= |z| \cdot |z^2 - w\alpha + \alpha^2| \\ &\leq a^3\exp(-3bw) + a\exp(-bw)(\alpha^2 + \alpha w). \end{aligned}$$

Also, we have

$$\begin{aligned} w' &\leq w(z^2 + \alpha^2) + 4z^2\alpha \\ &\leq (w + 4\alpha)a^2\exp(-2bw) + w\alpha^2. \end{aligned}$$

Hence,

$$\begin{aligned} & a\exp(-bw') > |z'| \\ \Leftarrow\ & a\exp\Big(-b\big((w+4\alpha)a^2\exp(-2bw) + w\alpha^2\big)\Big) > a^3\exp(-3bw) + a\exp(-bw)(\alpha^2 + \alpha w) \\ \Leftarrow\ & \exp\Big(-b(w+4\alpha)a^2\exp(-2bw)\Big)\cdot\exp(-\alpha^2 bw) > a^2\exp(-3bw) + \exp(-bw)(\alpha^2 + \alpha w) \\ \Leftarrow\ & \exp\Big(-b(w+4\alpha)a^2\exp(-2bw)\Big) > a^2\exp((\alpha^2-3)bw) + \exp((\alpha^2-1)bw)(\alpha^2 + \alpha w) \\ \Leftarrow\ & 1 + b(w+4\alpha)a^2\exp(-2bw) > a^2\exp((\alpha^2-3)bw) + \exp((\alpha^2-1)bw)(\alpha^2 + \alpha w). \end{aligned} \tag{18}$$

Let

$$p(w) = 1 + b(w+4\alpha)a^2\exp(-2bw),\ q(w) = a^2\exp((\alpha^2-3)bw) + \exp((\alpha^2-1)bw)(\alpha^2+\alpha w).$$

Note that

$$p'(w) = a^2 b \exp(-2bw)\Big(1 - 2b(w + 4\alpha)\Big)$$
$$\propto -2bw + 1 - 8\alpha b.$$

Therefore $p(w)$ increases from $(-\infty, w_0)$ for some $w_0 \in \mathbb{R}$ and decreases on $[w_0, +\infty)$. Since $\lim_{w\to+\infty} p(w) = 1$, we have that

$$\min_{w\in[0,+\infty)} p(w) = \min\{p(0), 1\} = \min\{1 + 4a^2 b\alpha, 1\} = 1.$$

Note also that

$$q'(w) = \exp((\alpha^2 - 1)bw)\Big(a^2(\alpha^2 - 3)b\exp(-2bw) + (\alpha^2 - 1)b(\alpha^2 + \alpha w) + \alpha\Big)$$
$$\propto a^2(\alpha^2 - 3)b\exp(-2bw) + (\alpha^2 - 1)b\alpha w + (\alpha^2 - 1)b\alpha^2 + \alpha.$$

Note, that $a^2(\alpha^2 - 3)b\exp(-2bw) < 0$ always holds. When b is large enough such that $(\alpha^2 - 1)b\alpha^2 + \alpha$ is negative,$(\alpha^2 - 1)b\alpha w + (\alpha^2 - 1)b\alpha^2 + \alpha$ is also negative. Hence,

$$\max_{w\in[0,+\infty)} q(w) = q(0) = a^2 + \alpha^2.$$

Since $0 < \alpha < 1$, we can always select a small enough such that $q(0) < 1$. Under such selection we have that $p(w) > q(w)$ holds for all $w \geq 0$ and hence (18) holds. Therefore, $\{|z| < a\exp(-bw)\}$ is forward invariant. Due to the exponential decay, we can always select a small enough and b large enough such that $\{|z| < a\exp(-bw)\} \subset \{Q(z, w) > Q(F(z, w))\}$, where the latter set is given in Lemma 12. Therefore, in this exponential cone, Q monotonically decays, and the orbit converges to the minimizer almost surely. This completes the proof. □

In the following, we show that when the initialization is near the boundary, the orbit can visit any point in the space.

Proposition 25. *Assume* $0 \leq \nu < \min\{\frac{1}{2}, 1 - |\mu|\}$. *Consider arbitrary point* $m_0 = (z, w) \in \Omega$. *When* $\mu \geq 0$, $\lim_{N\to\infty} G_0^N(m_0) = (-2 + \nu, 4 - 2(\nu + \mu))$. *When* $\mu < 0$, $\lim_{N\to\infty} G_2^N(m_0) = (2 - \nu, 4 + 2(\nu + \mu))$.

Proof. Let $(z', w') = F(z, w)$ and $m_k = G_0^k(m_0)$. Consider the function $E(z, w) = w + 2(z + \mu)$. We have

$$E(F(z, w)) - E(z, w) = w' + 2(z' + \mu) - w - 2(z + \mu)$$
$$= (w + 2(z + \mu))(z + \nu - 2)(z + \nu).$$

Note for $(z, w) \in \Omega$, $w + 2(z + \mu) \geq 0$. When $w > 2(z + \mu)$, we have that

$$E(F(z, w)) - E(z, w) > 0 \Leftarrow z < -\nu. \tag{19}$$

We have that $m_k \in \mathrm{cl}(A_0)$ for $k \geq 1$. Hence, the z-coordinate of m_k is smaller than $\nu - 1$ for all $k \geq 1$. Since $\nu < 1/2$, $\nu - 1 < -\nu$. Hence, $m_k \in \{E(F(z, w)) > E(z, w)\}$ for all $k \geq 1$. This implies that $E(m_k)$ monotonically decreases. Since E has lower bound 0 on Ω, $E(m_k)$ converges to some finite value E^*. For contradiction, assume m_k is unbounded. Note for any m_1, we have the set

$$\{E(z, w) \leq E(m_1)\} \cap \{|z| < M\}$$

is bounded for any $M > 0$. Hence, we have the z-coordinate of m_k tends to negative infinity. Note that for sufficiently small z and $(z, w) \in \Omega$, we have

$$w' > w \Leftrightarrow 4z(z + \mu)(-1 + \nu) + w(z^2 + (-2 + \nu)\nu) > 0$$
$$\Leftarrow w > \frac{4z(z + \mu)(1 - \nu)}{z^2 + (-2 + \nu)\nu}$$
$$\Leftarrow -2(z + \mu) > \frac{4z(z + \mu)(1 - \nu)}{z^2 + (-2 + \nu)\nu}$$
$$\Leftarrow -(z^2 + (-2 + \nu)\nu) < 2z(1 - \nu)$$
$$\Leftarrow z^2 + 2(1 - \nu)z + \nu(2 - \nu) > 0,$$

which clearly holds when z is sufficiently small. Therefore, m_k must lie in the region $\{w' > w\}$ for all $k \geq K$ for some finite $K > 0$. Note this implies that the w-coordinate of m_k starts to decrease from all $k \geq K$. This conflicts with the fact that m_k is unbounded. Hence m_k is bounded.

According to (19), m_k has to converge to

$$\mathrm{cl}(A_0) \cap \{(w + 2(z + \mu))(z + \nu - 2)(z + \nu) = 0\} = \{(w + 2(z + \mu) = 0\}.$$

Otherwise, assume $m_k \subset K$ for all k and some compact set K. The function $E(F(z, w)) - E(z, w)$ is uniform continuous, so if m_k does not converge to its zero set, $E(m_k) - E(m_{k-1})$ is bounded below and $E(m_k)$ can not converge.

Note, when restricting to $w = -2(z + \mu)$, the w-update is given by

$$w' = d(w) = w(\frac{w}{2} - 1 + \nu + \mu)^2.$$

Solving $d(w) = w$, we obtain that d has three fixed points, $0, -2(\mu + \nu)$ and $4 - 2(\mu + \nu)$. Note when $\mu \geq 0$, we have $-2(\mu + \nu) < 0$. Therefore, on $w \geq 0$, d has two fixed points. Note $d'(0) = (-1 + \mu + \nu)^2 < 1$ as $\mu + \nu < 1$, and hence $w = 0$ is repelling under d^{-1}. Note $d'(4 - 2(\mu + \nu)) = 5 - 2(\mu + \nu) > 1$, and hence $w = 4 - 2(\mu + \nu)$ is attracting under d^{-1}. With basic graph analyses, we have that $w = 4 - 2(\mu + \nu)$ globally attracts all orbits under d^{-1}, except the point $w = 0$. Notice that, one must have $m_1 \neq (-\mu, 0)$ as $m_1 \in \mathrm{cl}(A_1)$. Therefore, since m_k converges to $w = -2(z + \mu)$, we have that m_k converges to $(-2 + \nu, 4 - 2(\nu + \mu))$. The case of $y < 0$ can be proved via a analogous procedure. This completes the proof. □

Using Proposition 25, we show that for the gradient descent system, the converged minimizer is unpredictable when the initialization is near the boundary.

Proposition 26. *Consider $\xi_1 = (-2 + \nu, 4 - 2(\nu + \mu))$ and $\xi_2 = (2 - \nu, 4 + 2(\nu + \nu))$. For $i = 1, 2$, we have that $\cup_{N=0}^{\infty} F^{-N}(\xi_i)$ has infinitely many points and $\cup_{N=0}^{\infty} F^{-N}(\xi_i) \subset \partial T(\mathcal{D}_\eta'')$. When $y \geq 0$, for any open set O such that $O \cap \cup_{N=0}^{\infty} F^{-N}(\xi_1) \neq \varnothing$, there exists $(z', w'), (z'', w'') \in O$ such that, for any $(u', v'), (u'', v'')$ that satisfy $T(u', v') = (z', w')$ and $T(u'', v'') = (z'', w'')$, we have $\mathrm{GD}_\eta^N(u', v')$ converges $p^+(u', v')$ and $\mathrm{GD}_\eta^N(u'', v'')$ converges $p^-(u'', v'')$. When $y < 0$, the same result holds for any open set O such that $O \cap \cup_{N=0}^{\infty} F^{-N}(\xi_2) \neq \varnothing$.*

Proof. We present the proof for $y \geq 0$ for brevity. The case $y < 0$ can be proved via an analogous procedure. We first show that $\cup_{N=0}^{\infty} F^{-N}(\xi_i)$ has infinitely many points and $\cup_{N=0}^{\infty} F^{-N}(\xi_i) \subset \partial T(\mathcal{D}_\eta'')$. Notice that, ξ_1 lies in the set $\{(z, w) \in \Omega \colon w = -2(z + \mu)\}$. By Proposition 11, this set is invariant under F, where the w-update is given by

$$w' = w(\frac{w}{2} - 1 + \mu + \nu)^2.$$

By differentiation, we know $w = 4 - 2(\mu + \nu)$ is a repelling fixed point. Specifically, we claim that on any neighborhood of $4 - 2(\mu + \nu)$ there exists a point that converges to 0 and a point that diverges to infinity. Note w converging to zero corresponds to (z, w) converging to $(-\mu, 0)$, and to (u, v) converging to the saddle $(\mathbf{0}, \mathbf{0})$. Therefore, we have $\xi_1 \in \partial T(\mathcal{D}_\eta'')$. Note, $Q(\xi_1) = 8 - 4\nu > 6 - 4\nu$. Therefore, by Proposition 13, $F^{-1}(\xi_1)$ can be explicitly given by $\cup_{k=0,1,2} G_i(\xi_1)$, where G_i is a homeomorphism for all i. Therefore,

$$\cup_{N=0}^{\infty} F^{-N}(\xi_1) = \{G_{i_1} \circ G_{i_k}(\xi_1) \colon \forall k \geq 1, i_j \in \{0, 1, 2\}, \forall j\}. \tag{20}$$

By the construction of G_i, the cardinality of this set is infinity. Also, as each G_i is a homeomorphism, any point in this set belongs to $\partial T(\mathcal{D}_\eta'')$.

Next, we show that for any open set O such that $O \cap \cup_{N=0}^{\infty} F^{-N}(\xi_1) \neq \varnothing$, there exists $(z', w'), (z'', w'') \in O$ satisfy the claimed properties. Note, by (20), it suffices to prove this result for O that satisfies $O \ni \xi_1$. When $y \leq \lambda$, L has a unique minimizer $(\mathbf{0}, \mathbf{0})$ and the result obvious holds from Proposition 25. Now consider $y > \lambda$, in which case the set of global minimizers is given by $\left\{q = 0, \|p\|^2 = 2(y - \lambda)\right\}$. Consider $p = (u + v)/\sqrt{2}$ and $q = (u - v)/\sqrt{2}$. We have that

$$p_k = p_0 \Pi_{j=0}^{k-1}(1 - z_j - \nu).$$

Therefore, the orientation of p_∞ is fully determined by whether number of z_j such that $1 - z_j - \nu > 0$ is even or odd. Now let $m_* = (-\nu, 2(\mu - \nu))$ denote the minimizer. Note, the boundary $w = 2(z+\mu)$ is invariant by Lemma 11, where the w-update is given by

$$w' = d(w) = w(\frac{w}{2} - 1 - \mu + \nu)^2.$$

Solving $d(w) = 2(\mu - \nu)$ yields two solutions:

$$w_\pm = 2 + \mu - \nu \pm \sqrt{-4 + (-2 - \mu + \nu)^2}.$$

Note these roots are reals since $\mu - \nu > 0$. Note on the line $w = 2(z + \mu)$, $1 - \nu = z$ yields $w = 2(1 - \nu + \mu)$. Let $\alpha = \mu - \nu$. We have that

$$\begin{aligned} & 2(1+\alpha) < 2 + \alpha + \sqrt{(2+\alpha)^2 - 4} \\ \Leftrightarrow\ & \alpha < \sqrt{\alpha^2 + 4\alpha} \\ \Leftarrow\ & \alpha < 4, \end{aligned}$$

which is true since $0 < \nu, \mu < 1$. Similarly, we have

$$\begin{aligned} & 2(1+\alpha) > 2 + \alpha - \sqrt{(2+\alpha)^2 - 4} \\ \Leftrightarrow\ & \alpha > -\sqrt{\alpha^2 + 4\alpha}, \end{aligned}$$

which is true since $\alpha > 0$. Therefore, there exists $m_*^+, m_*^- \in \Omega$ such that, $F(m_*^\pm) = m^*$ and $m_*^+ \in \{z > 1 - \nu\}$ and $m_*^- \in \{z, 1 - \nu\}$. By Proposition 25, $G_0^N(m_*^\pm)$ converges to $(2 - \nu, 4 + 2(\nu + \mu))$. Notice that, for $N \geq 1$, $G_0^N(m_*^\pm) \in \{z < 1 - \nu\}$ since the image set of G_0 is $\mathrm{cl}(A_0)$. Therefore, the entire sequence $G_0^N(m_*^+)$ enters $\{z > 1 - \nu\}$ exactly one time. Similarly, the entire sequence $G_0^N(m_*^-)$ enters $\{z > 1 - \nu\}$ exactly zero time. Therefore, the corresponding uv-orbit converges the maximal and minimal distance solution. This completes the proof. □

E.2.2 Proof of Theorem 3

Proof of Theorem 3. In the quotient system F, the basin of attraction of the point $(-\mu, 0)$ has measure zero. This is because as in the proof for Proposition 22, the basin can be given by $\cup_{N=0}^\infty F^{-N}(O \cap \{w = -2\mathrm{sgn}(\mu)(z + \mu)\})$ for some neighborhood O of $(-\mu, 0)$. Since the Jacobian of F has full rank almost everywhere, this basin of attraction is a measure zero set. According to Proposition 6, any measure-zero event in system F corresponds to a measure-zero even in system GD_η. Therefore, $\mathcal{S}_\eta$ has measure zero. The projected boundary is self similar with degree three is directly given by Proposition 23. The unboundedness is given by Proposition 24.

Finally, we prove sensitivity to initialization. Consider any open neighborhood $W \subset \mathbb{R}^{2d}$ such that $W \cap \partial\mathcal{D}_\eta'' \neq \varnothing$. We claim that $T(W)$ is a neighborhood that contains an open neighborhood on $T(\partial\mathcal{D}_\eta'')$. Notice the Jacobian of the map T drops rank if and only if $u = \pm v$. If $W \cap \{u = \pm v\} = \varnothing$, then by constant rank theorem, T is locally a projection, which gives the claim. If $W \cap \{u = \pm v\} \neq \varnothing$, then without loss of generality, assume $W = B((u_0, u_0), \delta)$. Then $T(u_0, u_0) = (\|u_0\|^2, 2\|u_0\|^2)$. We show that for any point (z', w') that is sufficiently close to $(\|u_0\|^2, 2\|u_0\|^2)$, there exists a preimage under T in W. Note, as T is surjective, assume $T(u', v') = (z', w')$. Note whenever (z', w') tends to $(\|u_0\|^2, 2\|u_0\|^2)$, we have $w' + 2z' = \|u' + v'\|^2$ tends to $4\|u_0\|^2$ and $w' - 2z' = \|u' - v'\|^2$ tends to 0. Therefore, (u', v') tends to $\{u = v, \|u\| = \|u_0\|\}$. Note, the map T is invariant under rotation. Therefore, with proper rotation, (u', v') tends to $\{u = v, u = u_0\} = (u_0, u_0)$ and thus it lies in W. When $y \geq 0$, consider the set $H = T^{-1}(\cup_{N=0}^\infty F^{-N}(\xi_1))$, where ξ_1 is defined in Proposition 26. By Proposition 26, H has infinitely many elements. As shown in Proposition 23, we have $T(\partial\mathcal{D}_\eta'') = \partial T(\mathcal{D}_\eta'')$. Hence, $\cup_{N=0}^\infty F^{-N}(\xi_1) \subset \partial T(\mathcal{D}_\eta'') = T(\partial\mathcal{D}_\eta'')$. Therefore, when $W \cap H \neq \varnothing$, $T(W)$ is a neighborhood that intersects with $\cup_{N=0}^\infty F^{-N}(\xi_1)$. By Proposition 26, there exist $\theta', \theta'' \in W$ such that $\mathrm{GD}_\eta^N(\theta')$ converges to $p^+(\theta')$ and $\mathrm{GD}_\eta^N(\theta'')$ converges to $p^-(\theta')$. The case of $y < 0$ can be proved analogously using Proposition 26. This completes the proof. □

F Non-existence of continuous dynamical invariant

Consider the scalar factorization problems:

$$\min_{\theta=(u,v)} L(\theta) = \frac{1}{2}(uv - y)^2 + \frac{\lambda}{2}(u^2 + v^2), \tag{21}$$

where $\lambda \geq 0$ and $u, v, y \in \mathbb{R}$. We show that there is no simple quantity that remains invariant during training.

A *dynamical invariant* is a map defined on the parameter space of the model whose values remain unchanged along optimization trajectories. Formally, for gradient descent applied to problem (21), a map $I(u, v) \colon \mathbb{R}^2 \to \mathbb{R}^k$ with $k \geq 1$ is a δ-approximate invariant if $\|I(\mathrm{GD}^N(\bar{u}, \bar{v})) - I(\bar{u}, \bar{v})\| \leq \delta$ holds for all $N \geq 1$ and initializations $(\bar{u}, \bar{v}) \in \mathbb{R}^{2d}$, where $\|\cdot\|$ is a norm on $\mathbb{R}^k$. When $\delta = 0$, I becomes a strict invariant. Invariants and approximate invariants have been used extensively to analyze the optimization dynamics of gradient flow and gradient descent in non-convex optimization problems. Particularly, for problem (1) without regularization, the imbalance $I(U, V) = UU^\top - VV^\top$ is a well-known invariant of gradient flow (Du et al., 2018) and an approximate invariant of gradient descent with small step sizes (Arora et al., 2019; Ye and Du, 2021; Xu et al., 2023). In contrast, the following result shows that no simple invariants exist under large step sizes.

Theorem 27 (Non-Existence of Simple Dynamical Invariants)**.** *Consider gradient descent with step size η applied to problem* (21) *with $0 \leq \lambda < \min\{(1/\eta) - |y|, 1/(2\eta)\}$. If $I(u, v) \colon \mathbb{R}^2 \to \mathbb{R}^k$ is a continuous δ-approximate invariant, then $\sup_{(u,v),(u',v') \in \mathbb{R}^2} \|I(u, v) - I(u', v')\| \leq 2\delta$. Consequently, the only continuous invariants are the constant functions.*

Proof. We use the notation F, μ, ν, z, w as stated in the conjugacy (7). Assume I is a continuous δ-approximate invariant. For any $\varepsilon > 0$, there exist θ', θ'' such that

$$\|I(\theta') - I(\theta'')\| > \sup_{(u,v),(u',v') \in \mathbb{R}^2} \|I(u, v) - I(u', v')\| - \varepsilon.$$

Without loss of generality, assume $y \geq 0$. Now fix any point $\theta \in T^{-1}(\lambda - 2/\eta, 4/\eta - 2(y + \lambda))$. Under the conjugacy (7), we have that $T(\theta) = (\nu - 2, 4 - 2(\mu + \nu))$. Then according to Proposition 25 for the regularized case and Proposition 20, in any neighborhood O of $T(\theta)$, there exists ξ', ξ'' and N', N'' such that $F^{N'}(\xi') = T(\theta')$ and $F^{N''}(\xi'') = T(\theta'')$. Using the same argument as in Appendix E.2.2 and in Appendix E.1.2, we have that there exists $\bar{\theta}', \bar{\theta}''$ such that $T(\mathrm{GD}_\eta^{N'}(\bar{\theta}')) = T(\theta')$ and $T(\mathrm{GD}_\eta^{N''}(\bar{\theta}'')) = T(\theta'')$. Next, we show that $\bar{\theta}'$ and $\bar{\theta}''$ can be chosen such that $\mathrm{GD}_\eta^{N'}(\bar{\theta}') = \theta'$ and $\mathrm{GD}_\eta^{N''}(\bar{\theta}'') = \theta''$. To see this, notice that, for any $(u, v), (s, t) \in \mathbb{R}^2$, $(u, v) = (s, t)$ if and only if $T(u, v) = T(s, t)$ and the two pairs, $u + v$ and $s + t$, and, $u - v$ and $s - y$, have the same sign. Consider change of coordinate $p = (u + v)/\sqrt{2}$ and $q = (u - v)/\sqrt{2}$. Let $p_k = (u_k, v_k)$ denote the orbit under GD_η. By direct computation, we have that

$$p_k = p_0 \Pi_{j=0}^{k-1}(1 - z_j - \nu).$$

Therefore, the sign of $p_{N'}$ is fully determined by whether number of z_j such that $1 - \nu > z_j$ is even or odd. We denote this number by n_p. Similarly, we have

$$q_k = q_0 \Pi_{j=0}^{k-1}(1 + z_j - \nu),$$

and the sign of $q_{N'}$ is fully determined by whether number of z_j such that $z_j > \nu - 1$ is even or odd. We denote this number by n_q. Notice that we can take ξ' as follows

$$\xi' = G_0^{m_p} \circ G_2^{m_q}(T(\theta')),$$

here $m_q \in \{0, 1\}$, and m_p is any large enough integer. Note since the image of G_0 lies out side $\{z > 1 - \nu\}$, m_p does not have an effect on n_q. Also, since the image of G_2 is contained in $\{z > 1 - \nu\}$, one can always select m_q from $\{0, 1\}$ to make n_q even or odd. Meanwhile, since the image of G_0 is contained in $\{z < \nu - 1\}$, one can always select a m_p to make n_p even or odd. Therefore, the sign of $p_{N'}$ and $q_{N'}$ can be arbitrary. This implies that, one can always select $\bar{\theta}'$ such that $\mathrm{GD}_\eta^{N'}(\bar{\theta}') = \theta'$. A similar statement holds for $\bar{\theta}''$.

Since I is δ-invariant, we have:

$$\|I(\bar{\theta}') - I(\bar{\theta}'')\| > \|I(\theta') - I(\theta'')\| - 2\delta > \sup_{(u,v),(u',v') \in \mathbb{R}^2} \|I(u, v) - I(u', v')\| - \varepsilon - 2\delta.$$

Notice that $\bar{\theta}', \bar{\theta}''$ can be arbitrarily close to θ. Since I is continuous at θ and ε is arbitrary, we have that

$$\sup_{(u,v),(u',v') \in \mathbb{R}^2} \|I(u, v) - I(u', v')\| \leq 2\delta,$$

which completes the proof.

□

G GENERAL MATRIX FACTORIZATION

We present the extensions of the results in Section 3 to general matrix factorization.

In the following, we present the extension of Theorem 1 to unregularized matrix factorization.

Theorem 28 (Unregularized Matrix Factorization)**.** *Consider gradient descent with step size η applied to problem* (1) *with $\lambda = 0$ and $d \geq d_y$. Let $Y = \mathrm{Diag}(y_1 \cdots, y_{d_y})$. Consider the set*

$$\mathcal{W} = \left\{(U,V) \in \mathbb{R}^{2d \cdot d_y} \colon \ \langle u^i, u^j \rangle = \langle u^i, v^j \rangle = \langle v^i, v^j \rangle = 0, \ \forall i \neq j \right\}, \tag{22}$$

where u^i, v^i denote the ith column of matrices U, V. Assume the initialization $(\bar{U}, \bar{V}) \in \mathcal{W}$. The following holds:

- ***Critical Step Size**: Define the critical step size*

$$\eta^*(\bar{U}, \bar{V}) = \min_i \min \left\{ \frac{1}{|y_i|}, \ \frac{8}{\|\bar{u}^i\|_2^2 + \|\bar{v}^i\|_2^2 + \sqrt{(\|\bar{u}^i\|_2^2 + \|\bar{v}^i\|_2^2)^2 - 16 y_i ((\bar{u}^i)^\top \bar{v}^i - y_i)}} \right\}.$$

  For almost all initializations (under surface measure on $\mathcal{W}$), the algorithm converges to a global minimum if $\eta < \eta^*(\bar{U}, \bar{V})$, and it does not converge to a global minimum if $\eta > \eta^*(\bar{U}, \bar{V})$. Therefore, when η satisfies $\eta \|Y\|_2 < 1$, the convergence region restricted to $\mathcal{W}$, $\mathcal{D}_\eta \cap \mathcal{W}$, is equal almost everywhere (under surface measure on $\mathcal{W}$) to the following set:

$$\mathcal{D}'_\eta = \left\{ (U,V) \in \mathcal{W} \colon \|u^i\|_2^2 + \|v^i\|_2^2 + \sqrt{(\|u^i\|_2^2 + \|v^i\|_2^2)^2 - 16 y ((u^i)^\top v^i - y_i)} < \frac{8}{\eta}, \ \forall i \right\}.$$

- ***Sensitivity to Initialization**: Fix a step size η that satisfies $\eta \|Y\|_2 < 1$. Given arbitrary $\theta \in \partial \mathcal{D}'_\eta$ (here boundary is taken with respect to the subspace topology on $\mathcal{W}$), $\varepsilon > 0$ and $K_1, K_2 > 0$, there exist $\theta', \theta'', \theta''' \in B(\theta, \varepsilon)$ such that, as N tends to infinity, $\mathrm{GD}_\eta^N(\theta')$ converges to a global minimizer with norm larger than K_1, $\mathrm{GD}_\eta^N(\theta'')$ converges to a global minimizer with $\|UU^\top - VV^\top\|_F > K_2$, and $\mathrm{GD}_\eta^N(\theta''')$ converges to a stationary point, which is saddle point when $\min\{|y_i|\} > 0$.*

- ***Trajectory Complexity**: Assume $\eta \|Y\|_2 < 1$. The topological entropy of the gradient descent system GD_η satisfies $h(\mathrm{GD}_\eta) \geq \log 3$. Moreover, GD_η has periodic orbits of any positive integer period.*

All of the above results follow directly from Theorem 1 and Proposition 5. We remark that, for a dynamical system $F \colon X \to X$, if $S \subset X$ is an invariant set, i.e., $F(S) \subset S$, then we have $h(F) \geq h(F|_S)$. This gives the result for topological entropy.

We now present the extensions of Theorem 3 and Theorem 4 to regularized matrix factorization.

Theorem 29 (Regularized Matrix Factorization)**.** *Consider gradient descent with step size η for problem* (4)*. Let $Y = \mathrm{Diag}(y_1 \cdots, y_{d_y})$. Assume that $0 < \lambda \leq \min_{i=1,\cdots,d_y} \{(1/\eta) - |y_i|, 1/(2\eta)\}$. Let $\mathcal{W}$ be defined as in* (22)*. Assume the initialization $(\bar{U}, \bar{V}) \in \mathcal{W}$. Consider the map $T_i(U,V) = ((u^i)^\top v^i, \|u^i\|_2^2 + \|v^i\|_2^2)$. Let $\mathcal{S}_\eta$ denote the set of initializations (U,V) that converges to $(\mathbf{0}, \mathbf{0})$. Let $\mathcal{D}''_\eta = \mathcal{D}_\eta \cup \mathcal{S}_\eta$. The following holds:*

- ***Self-similarity:** For any $i \in \{1, \cdots, d_y\}$, $T_i(\partial(\mathcal{D}''_\eta \cap \mathcal{W}))$ is self-similar with degree three (here boundary is taken with respect to the subspace topology on $\mathcal{W}$).*

- ***Unboundedness**: When $Y = 0$, there exist constants $a, b > 0$ such that almost all initializations $(\bar{U}, \bar{V}) \in \mathcal{W}$ (under surface measure on $\mathcal{W}$) with $|(\bar{u}^i)^\top \bar{v}^i| < a \exp(-b(\|\bar{u}^i\|_2^2 + \|\bar{v}^i\|_2^2))$ for all $i \in \{1, \cdots, d_y\}$ converge to a global minimizer.*

- ***Sensitivity to Initialization**: Let $(u_t^i, v_t^i)_{t \geq 0}$ denote the gradient descent trajectory of the pair (u^i, v^i), with $(u_0^i, v_0^i) = (\bar{u}^i, \bar{v}^i)$. Let $\mathcal{M}_i$ denote the set of global minimizers for the scalar problem $L_i(u,v) = \frac{1}{2}(u^\top v - y_i)^2 + \frac{\lambda}{2}(\|u\|_2^2 + \|v\|_2^2)$. Then $\mathcal{M} \cap \mathcal{W} = \mathcal{M}_1 \times \cdots \times \mathcal{M}_{d_y}$, where*

$\mathcal{W}$ denotes the set of global minimizers for problem (4)*. We have that, for any $(U, V) \in \mathcal{D}_\eta \cap \mathcal{W}$ and any $i \in \{1, \cdots, d_y\}$, as t tends to infinity, (u_t^i, v_t^i) converges either to*

$$p^-(u_0^i, v_0^i) = \arg \min_{(u,v)\in\mathcal{M}_i} \|(u, v) - (u_0^i, v_0^i)\|^2,$$

or to

$$p^+(u_0^i, v_0^i) = \arg \max_{(u,v)\in\mathcal{M}_i} \|(u, v) - (u_0^i, v_0^i)\|^2.$$

Moreover, there exist infinitely many points on $\partial(\mathcal{D}''_\eta \cap \mathcal{W})$ (here boundary is taken with respect to the subspace topology on $\mathcal{W}$) such that for any open set O containing such a point, there exist $i \in \{1, \cdots, d_y\}$, $(U', V'), (U'', V'') \in O$ such that, as t tends to infinity, $(u_t^{i,\prime}, v_t^{i,\prime})$ converges to $p^-(u_0^{i,\prime}, v_0^{i,\prime})$ and $(u_t^{i,\prime\prime}, v_t^{i,\prime\prime})$ converges to $p^+(u_0^{i,\prime\prime}, v_0^{i,\prime\prime})$.

- ***Stable Dynamics Under Small Step Size****: Consider the function*

$$Q(u, v) = \|u\|_2^2 + \|v\|_2^2 + \sqrt{(\|u\|_2^2 + \|v\|_2^2)^2 - 16y(u^\top v - y)}.$$

Then the following holds for almost all initializations $(\bar{U}, \bar{V}) \in \mathcal{W}$ (under surface measure on $\mathcal{W}$): If $\eta < \min_{i=1,\cdots,d_y} 8/(4\lambda + Q(\bar{u}^i, \bar{v}^i))$, then gradient descent converges to a global minimizer; If $\eta < \min_{i=1,\cdots,d_y} 4/(4\lambda + Q(\bar{u}^i, \bar{v}^i))$, then for all i, (u_t^i, v_t^i) converges to $p^-(u_0^i, v_0^i)$.

All of the above results follow directly from Theorem 3, Theorem 4 and Proposition 5. We remark that, while the above Theorems are presented for initializations in $\mathcal{W}$, chaotic phenomena are observed under generalization initializations. Experiments are provided in Appendix I.

In the following, we present the proof of Proposition 5.

Proof of Proposition 5. Recall the update:

$$U_{t+1} = U_t - \eta V_t(V_t^\top U_t - Y^\top) - \eta\lambda U_t, \quad V_{t+1} = V_t - \eta U_t(U_t^\top V_t - Y) - \eta\lambda V_t.$$

For $(U_t, V_t) \in \mathcal{W}$, we have that

$$\begin{aligned} U_{t+1} &= U_t - \eta V_t V_t^\top U_t + \eta V_t Y^\top - \eta\lambda U_t \\ &= U_t - \eta \sum_{k=1}^{d_y} v_t^k (v_t^k)^\top \cdot U_t + \eta V_t Y^\top - \eta\lambda U_t. \end{aligned}$$

Therefore, for $j = 1, \cdots, d_y$,

$$\begin{aligned} u_{t+1}^j &= u_t^j - \eta \sum_{k=1}^{d_y} v_t^k (v_t^k)^\top u_t^j + \eta y_j v_t^j - \eta\lambda u_t^j \\ &= u_t^j - \eta v_t^j (v_t^j)^\top u_t^j + \eta y_j v_t^j - \eta\lambda u_t^j \\ &= u_t^j - \eta\big((v_t^j)^\top u_t^j - y_j\big) v_t^j - \eta\lambda u_t^j. \end{aligned}$$

Therefore, the one-step u^j-update aligns with that in scalar factorization problem. Similarly, we can show this holds for v^j-update. Now it suffices to verify that $\mathcal{W}$ is forward invariant. Assume $(U_t, V_t) \in \mathcal{W}$. Notice that both u_{t+1}^j and v_{t+1}^j are linear combinations of u_t^j and v_t^j. Then it clear that

$$\langle u_{t+1}^j, u_{t+1}^k \rangle = \langle u_{t+1}^j, v_{t+1}^k \rangle = \langle v_{t+1}^j, v_{t+1}^k \rangle = 0$$

whenever $j \neq k$. This completes the proof. □

The gradient descent update map GD_η is non-invertible in general. Nevertheless, we show that the parameter space can be partitioned into small pieces, so that confined on each piece, GD_η has a simple behavior.

Proposition 30. *Let $\mathrm{GD}_\eta \colon \mathbb{R}^{2d\cdot d_y} \to \mathbb{R}^{2d\cdot d_y}$ be the gradient descent update map for problem* (1)*. There exists a measure-zero set $\mathcal{K}_\eta \subset \mathbb{R}^{2dr}$ that satisfies: (i) $\mathcal{K}_\eta$ contains the critical points of GD_η; and (ii) $\mathbb{R}^{2dr} \setminus \mathcal{K}_\eta$ has finitely many connected components such that the restriction of GD_η to each component is a covering map.*

Proof. Note GD_η is clearly a non-constant polynomial map. By Jelonek (2002), there exists a semi-algebraic measure-zero set $S \subset \mathbb{R}^{2d\cdot d_y}$ such that, $\mathrm{GD}_\eta \colon \mathbb{R}^{2d\cdot d_y} \setminus \mathrm{GD}_\eta^{-1}(S) \to \mathbb{R}^{2d\cdot d_y} \setminus S$ is a proper map. Note $\det J\mathrm{GD}_\eta$ is a non-constant polynomial, so its zero locus is a semi-algebraic measure-zero set. Let $S' = \mathrm{GD}_\eta(\{\det J\mathrm{GD}_\eta = 0\})$ denote the set of critical values of GD_η, which has measure-zero by Sard's theorem and is also semi-algebraic. By Ponomarev (1987), the preimage of any measure-zero set has measure zero. In particular, $\mathcal{K}_\eta = \mathrm{GD}_\eta^{-1}(S) \cup \mathrm{GD}_\eta^{-1}(S')$ is a measure-zero and semi-algebraic set. Now consider $G = \mathrm{GD}_\eta|_{\mathbb{R}^{2d\cdot d_y}\setminus\mathcal{K}_\eta} \colon \mathbb{R}^{2d\cdot d_y} \setminus \mathcal{K}_\eta \to \mathbb{R}^{2d\cdot d_y} \setminus (S \cup S')$. Note, $\mathbb{R}^{2d\cdot d_y} \setminus \mathcal{K}_\eta$ has finitely many connected components since $\mathcal{K}_\eta$ is semi-algebraic. Let $\mathcal{C}$ be any connected component. By construction, $G|_{\mathcal{C}}$ is a proper map between connected manifolds that has full-rank Jacobian everywhere. To see this, let K be a compact set in $\mathbb{R}^{2d\cdot d_y} \setminus (S \cup S')$. Then K is compact in $\mathbb{R}^{2d\cdot d_y} \setminus S$ and $G^{-1}(K) = (F|_{\mathbb{R}^{2d\cdot d_y}\setminus F^{-1}(S)})^{-1}(K)$ is compact. Hence, $G|_{\mathcal{C}}$ is a smooth covering map (see, e.g., Lee, 2012). This completes the proof. □

H Experiment details

For Figure 1 left panel, we consider the problem $L(u, v) = (u^\top v - 1)^2 + 0.3(\|u\|_2^2 + \|v\|_2^2)$ with $(u, v) \in \mathbb{R}^{10}$. We randomly sampled two orthogonal unit vectors in $\mathbb{R}^{10}$. Viewing the two vectors as new axes, we evenly sampled 600^2 initial points in the range $[-4, 4]^2$. We then ran gradient descent with step size 1 for 1000 iterations. The training stops if the loss is below $L_{\min} + 10^{-6}$, where $L_{\min}$ is the global minimum or if it is above 100. For Figure 1 right panel, we consider $L(x, y) = (xy - 1)^2$ with $(x, y) \in \mathbb{R}^2$. We evenly sampled 800^2 initial points in the range $[-4.5, 4.5]^2$. We ran gradient descent with step size 0.2 for 6 iterations and recorded the final squared distances to the two minimizers, $m_1 = (1, 1)$ and $m_2 = (2.9, 1/2.9)$. Viewing the final distances as functions of the initial point, we used the "contourf" function from the Matplotlib package (version 3.5.2) to draw the sublevel sets of the distances. For the minimizer m_1, we drew the sublevel set of $[0, 0.15)$ to get the preimage of $\mathrm{GD}^{-6}(B(m_1, \sqrt{0.15}))$. For the minimizer m_2, we drew the sublevel set of $[0, 0.25)$ to get the preimage of $\mathrm{GD}^{-6}(B(m_2, \sqrt{0.25}))$.

For Figure 2, we consider $L(x, y) = (xy - 1)^2$ with $(x, y) \in \mathbb{R}^2$. For the left panel, we evenly sampled 800^2 initial points in the range $[-4.5, 4.5]^2$ and ran gradient descent with step size 0.2 for 6 iterations. To visualize the basin for unstable minimizers, note, as shown in the proof of Proposition 15, converging to unstable minimizers can only occur within finitely many steps. We therefore recorded the final loss value and used the "contour" function from the Matplotlib package (version 3.5.2) to collect points in the level set of 0 for the loss. Those points correspond to convergence to a global minimizer within 6 or less steps. We then filtered out and visualized points that converge to an unstable global minimizer, i.e., a minimizer with squared norm larger than $2/\eta$ (see Corollary 16).

In Figure 2, to visualize the basin for the saddle $(\mathbf{0}, \mathbf{0})$, note, as shown in the proof of Proposition 15, this basin can be given by $\cup_{N=0}^{\infty} F^{-N}(O \cap \{u = -\mathrm{sgn}(y)v\})$ for some neighborhood of $(\mathbf{0}, \mathbf{0})$. Then we also recorded the final distance to the set $\{u = -v\}$ and used the "contour" function from the Matplotlib package (version 3.5.2) to collect points in the level set of 0 for the distance. Then we filtered out the points that lie in $\mathcal{D}'_\eta$ (as defined in Theorem 1). This yield the basin associated with the saddle. To justify this procedure, note, as shown in Proposition 14, any point outside $\mathcal{D}'_\eta$ either converges to a minimizer within finite steps or diverges. Also note, by the analysis in Lemma 11, points on $\{u = -\mathrm{sgn}(y)v\}$ either converge to the saddle or diverge. For the right panel of Figure 2, we evenly sampled 800^2 points in $[-0.9, -0.6] \times [-4.55, -4.25]$. We ran gradient descent with step size 0.2 for 250 iterations. The training stops if the loss value is below 10^{-8} or above 100.

For Figure 3, we consider $L(u, v) = (uv - 0.5)^2/2 + 0.1(u^2 + v^2)$ where $(u, v) \in \mathbb{R}^2$. For the left panel, we consider the dynamical system defined by F (see Proposition 2) with $\eta = 1, \lambda = 0.2$ and $y = 1$. In the zw-space, we evenly sampled 2000^2 intial points in $[-2.5, 3] \times [0, 10]$ and filtered out those in $\{w \geq 2|z|\}$. We applied F^{200} to those sampled points and filtered out initial points that lead to loss value below $L_{\min} + 10^{-5}$ where $L_{\min}$ is the global minimum of L. Those points come from the projected convergence region $T(\mathcal{D}''_\eta)$. Then we used the "ndimage.binary_erosion" function from the SciPy package (version 1.9.1) to find the boundary of those points. The coloring of the boundary is based on the preimage structure of F, which is described in Proposition 13. For the middle panel, we evenly sampled 800^2 initial points in $[-4, 4]^2$ and ran gradient descent for 100 iterations. For the right panel, we estimated the box-counting dimension for the boundary points found in the left panel.

We first normalized these points to fit within $[0, 1]^2$. We then computed the number of boxes $N(\epsilon)$ needed to cover all the points, with the box width ε ranging from $1/2^2$ to $1/2^8$. We then performed linear regression on $\log N(\varepsilon)$ versus $\log(1/\varepsilon)$.

I ADDITIONAL EXPERIMENTS

How convergence boundary and basin of saddle evolve with λ In Figure 4, we illustrate how the convergence boundary and the basin of attraction of the saddle point evolve as the regularization parameter λ increases in scalar factorization problem. As shown in the figure, and consistent with our theoretical results, the boundary is smooth (in the almost everywhere sense) when $\lambda = 0$. When λ is just above zero, the boundary is close to a smooth and bounded set, with the fractal spikes so thin that they are barely visible. As λ increases, the fractal structure becomes more pronounced, and the spikes gradually get wider. Also, the basin of attraction of the saddle does not separate points inside the convergence region from points outside.

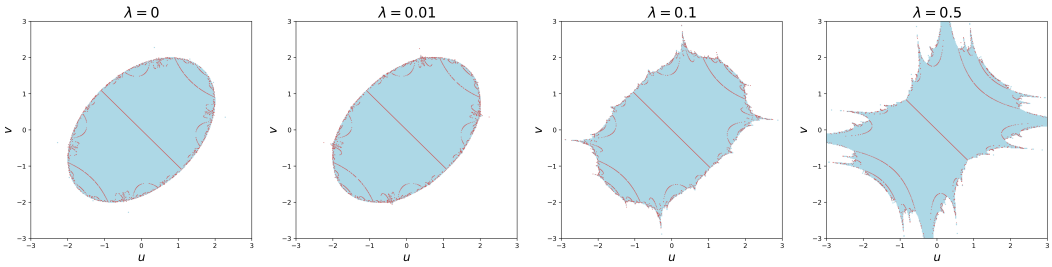

Figure 4: Gradient descent is applied to $L(u, v) = (uv - 0.8)^2/2 + \frac{\lambda}{2}(u^2 + v^2)$, where $u, v \in \mathbb{R}$ and $\lambda \in \{0, 0.01, 0.1, 0.5\}$. Blue points represent initializations that converge to a global minimizer; uncolored points represent initializations that do note converge. Red lines represent the basin of attraction of the saddle point $(0, 0)$.

Unregularized matrix factorization with general initialization In Figure 5, we ran gradient descent for shallow matrix factorization without regularization under general initialization. We observe that, on a random slice of the parameter space, the convergence boundary is non-smooth, suggesting that a smooth convergence boundary is a special property of the invariant subspace $\mathcal{W}$. This also implies that, globally, the critical step size might depend intricately on the initialization. However, sensitivity to initialization is common: on all the random slices, the converged minimizer is unpredictable near the convergence boundary. This suggests that chaotic dynamics always exists near the global convergence boundary.

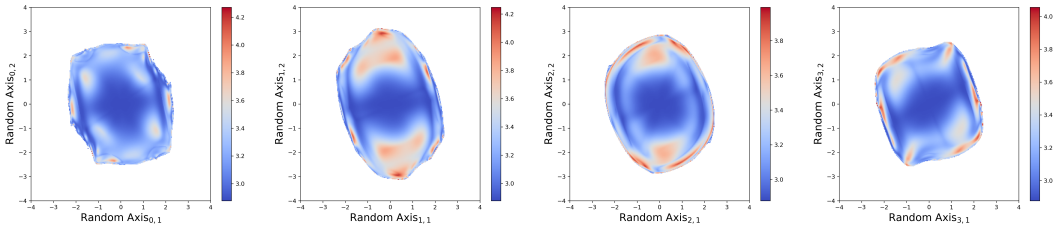

Unregularized

Figure 5: Gradient descent is applied to $L(U, V) = \|U^\top V - Y\|_F^2/2$, where $U, V \in \mathbb{R}^{5\times 4}$ and Y is a diagonal matrix whose diagonal elements are randomly sampled from $[0, 1]$. Four randomly sampled two-dimensional slices of the parameter space $\mathbb{R}^{40}$ are shown. The points are colored according to the squared Frobenius norm of the converged minimizer; uncolored points represent initializations that do not converge.

Regularized matrix factorization with general initialization In Figure 6, we ran gradient descent for shallow matrix factorization with regularization under general initialization. We observe that in the random slices of the parameter space, the convergence boundary exhibits fractal-like geometry,

although it appears to be less spiky than the boundary in scalar factorization. Also, as shown in the figure, sensitivity to initialization persist under general initialization. Together, Figure 6 and Figure 5 suggest that chaos and unpredictability are global properties of gradient descent in shallow matrix factorization.

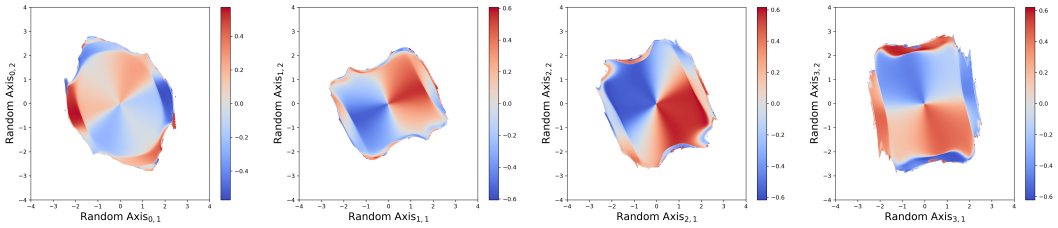

Regularized

Figure 6: Gradient descent is applied to $L(U, V) = \|U^\top V - Y\|_F^2/2 + 0.25(\|U\|_F^2 + \|V\|_F^2)$ where $U, V \in \mathbb{R}^{5\times 2}$ and $Y = \mathrm{Diag}(0.9, 0.8)$. Four randomly sampled two-dimensional slices of the parameter space $\mathbb{R}^{20}$ are shown. The points are colored according to the one coordinate value of the converged minimizer; uncolored points represent initializations that do not converge.

Deep matrix factorization In Figure 7, we ran gradient descent in depth-three matrix factorization under generalization initialization. For deep matrix factorization we observe that already for the unregularized problem, the convergence boundary exhibits fractal-like structure, as fine-scale structures emerge. We report how the squared norm of the converged minimizer depends on the initialization, for two random slices of the parameter space. As shown in the figure, while points near the origin converge to minimizers of small norm, sensitivity to initialization occurs in the vicinity of the boundary. For the regularized problem, we observe that not only the convergence boundary has a fractal-like structure, but the convergence region also becomes disconnected, with intricate connected components. The disconnectedness can be explained by the emergence of local minimizers, which attracts nearby trajectories, and non-strict saddles, which trap trajectories for long periods before they escape. For a detailed discussion of the landscape geometry of regularized deep matrix factorization, see Chen et al. (2025). Additionally, we observe sensitivity to initialization near the convergence boundary.

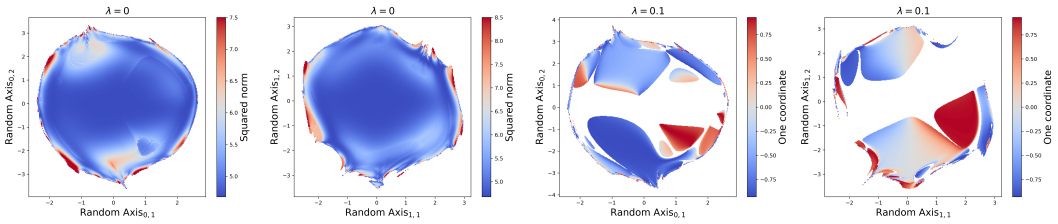

Unregularized Regularized

Figure 7: Gradient descent is applied to $L(U, V, W) = \|UVW - Y\|_F^2/2 + \frac{\lambda}{2}(\|U\|_F^2 + \|V\|_F^2 + \|W\|_F^2)$, where $U, V, W \in \mathbb{R}^{2\times 2}$ and $Y = \mathrm{Diag}(0.9, 0.5)$. The left two panels show two randomly sampled two-dimensional slices of the parameter space $\mathbb{R}^{12}$ for the unregularized problem. Points are colored according to the squared norm of the converged minimizer. The right two panels show the same random slices for the regularized problem. Points are colored according to one coordinate of the converged minimizer. In all panels, uncolored points represent initializations that do not converge to a global minimizer.